Use of porphyry indicator zircons (PIZs) in the sedimentary record as an exploration tool for covered porphyry copper deposits in the Atacama Desert, Chile

Héctor Pizarro, Sonia Rousse, Farhad Bouzari, Thomas Bissig, Michel Grégoire, Sébastien Carretier, Brian Townley, Guilhem Hoareau, Constantino Mpodozis

Use of porphyry indicator zircons (PIZs) in the sedimentary record as an exploration tool for covered porphyry copper deposits in the Atacama Desert, Chile

Héctor Pizarro, Sonia Rousse, Farhad Bouzari, Thomas Bissig, Michel Gregoire, Rodrigo Riquelme, Sébastien Carretier, Brian Townley, Guilhem Hoareau, Constantino Mpodozis

PII: S0375-6742(23)00198-X

DOI: https://doi.org/10.1016/j.gexplo.2023.107351

Reference: GEXPLO 107351

To appear in: *Journal of Geochemical Exploration*

Received date: 7 March 2023

Revised date: 14 September 2023

Accepted date: 12 November 2023

Please cite this article as: H. Pizarro, S. Rousse, F. Bouzari, et al., Use of porphyry indicator zircons (PIZs) in the sedimentary record as an exploration tool for covered porphyry copper deposits in the Atacama Desert, Chile, *Journal of Geochemical Exploration* (2023), https://doi.org/10.1016/j.gexplo.2023.107351

Use of Porphyry Indicator Zircons (PIZs) in the Sedimentary Record as an Exploration Tool for Covered Porphyry Copper Deposits in the Atacama Desert, Chile

Héctor Pizarro [a, *], Sonia Rousse [b], Farhad Bouzari [c], Thomas Bissig [c, d], Michel Gregoire [b], Rodrigo Riquelme [e], Sébastien Carretier [b], Brian Townley [a, f], Guilhem Hoareau [g], Constantino Mpodozis [h]

[a] Departamento de Geología, FCFM, Universidad de Chile, Casilla 13518, Correo 21, Santiago, Chile.

[b] GET, Université de Toulouse, IRD, CNRS, UPS, 14 Avenue E. Belin, Toulouse, 31400, France.

[c] MDRU - Mineral Deposit Research Unit, Department of Earth, Ocean and Atmospheric Sciences, The University of British Columbia, 2020–2207 Main Mall, Vancouver, BC V6T 1Z4, Canada.

[d] Present address: Bissig Geoscience Consulting, 1750 Maple St., Vancouver, BC. V6J 3S6, Canada.

[e] Departamento de Ciencias Geológicas, Universidad Católica del Norte, Av. Angamos 0610, Antofagasta, Chile.

[f] Advanced Mining Technology Center (AMTC), FCFM, Universidad de Chile, Av. Tupper 2007, Santiago, Chile.

[g] Université de Pau et Pays de l'Adour, E2S UPPA, CNRS, TOTAL, LFCR, Pau, France.

[h] Antofagasta Minerals, Apoquindo 4001, Piso 18, Santiago, Chile.

** Corresponding author: Departamento de Geología, FCFM, Universidad de Chile, Casilla 13518, Correo 21, Santiago, Chile.*

E-mail address: hpizarro@ing.uchile.cl or h.pizarro.08@gmail.com (Héctor Pizarro)

Abstract

This work explores the potential of geochemical and petrographic characteristics of detrital zircons coming from the sedimentary record of the Centinela District in Northern Chile to identify the presence of buried porphyry copper deposits under a transported gravel cover. The sampled sedimentary section was recovered from the pit of the exotic copper deposit of El Tesoro, located approximately 2 and 4 km west of the Esperanza and Mirador porphyries, respectively. The sedimentary cover comprises four units, Tesoro II, Tesoro III, Arrieros and Recent gravels, deposited since the late Cenozoic in an arid continental environment dominated by alluvial fans. Except for the Tesoro III gravels, all other units contain exotic-Cu mineralisation. In order to interpret the geochemical footprint of the investigated zircons, the Porphyry Indicator Zircon (PIZ) concept (Pizarro et al., 2020) is used. A PIZ need to comply with each of the following geochemical values: Hf >8,750 (ppm), Ce/Nd >1, Eu/Eu* >0.4, 10,000×(Eu/Eu*)/Y >1, (Ce/Nd)/Y >0.01, Dy/Yb <0.3 and 0.1 < Th/U < 1. These zircons also have Ti <9 ppm and Ce/Ce* <100 and usually show euhedral morphologies characterised by prismatic forms of type {110}. The geochemical and petrographic characteristics of the PIZs collected in the gravels are similar to zircons from the nearby Mirador and Esperanza porphyries. The highest PIZ concentration coincides with the gravel horizons with exotic-Cu mineralisation. Therefore, the PIZs found in the sedimentary record are a potential tracer of adjacent copper porphyries and represent a promising exploration tool for this type of hidden ore deposits in challenging sediment-covered areas.

Keywords: *Northern Chile, Porphyry Indicator Zircon (PIZ), Atacama gravels, Porphyry copper deposits, Exotic copper deposits.*

1 Introduction

Porphyry copper deposits contribute significantly to the global economy by providing copper, molybdenum, gold, rhenium, and silver. However, discoveries of economically viable porphyry copper deposits have become increasingly rare in the last 20 years (Kelley et al., 2011). This is partly due to the challenge of locating buried porphyries under transported sediment, such as glacial till cover in British Columbia, Yukon Territory (Canada) and Alaska (USA) or alluvial gravel cover in the Atacama Desert (Chile and Peru). Classical evaluation tools used by mining companies involve drilling, soil geochemistry, and geophysical methods. However, alternative exploration methods, such as analysing the mineralogical characteristics contained in the sediments that hide ore deposits, could allow vectoring and focusing exploration to specific targets. Thus, alternative methods can reduce costs and increase the effectiveness of conventional exploration methods.

Collaborative projects between research institutions and the mining industry, such as those operated through the Australian Mineral Industry Research Association (AMIRA), the Laboratoire Mixte International Pédiment et Cuivre (LMI COPEDIM), or the Canada Mining Innovation Council (CMIC) have successfully shown the utility of mineral chemistry combined with geological mapping for porphyry exploration (Cooke et al., 2014b, 2017; Wilkinson et al., 2015; Pizarro et al., 2020; Lee et al., 2021). Classical provenance studies that consider the mineralogical and chemical composition of clastic sediments have been of great importance for vectoring to prospective areas (e.g., Townley et al., 2003; Surour et al., 2003; Scott et al., 2014); unfortunately, clastic material may undergo alteration during transport and sedimentation, as a result of weathering and diagenesis (e.g., Leeder, 2012). To determine the origin of the clastic material, the petrographic, geochemical, and radiometric characterisation of minerals resistant to transport,

sedimentation and reworking is crucial. The investigated minerals must be abundant at the source and have distinctive chemical compositions to be pertinent to the exploration of ore deposits covered by sediments. This approach has been successfully applied in exploring mineral deposits, including diamondiferous kimberlite pipes and base metal sulfides (Griffin and Ryan, 1995; Averill, 2001, 2011).

Zircon is a common accessory mineral in igneous rocks that retains its primary chemical and isotopic composition from the time of crystallisation (Chernak et al., 1997), providing chemical information related to the parental magma. In sedimentary environments, zircon resists weathering (Fedo et al., 2003; Yang et al., 2012). Additionally, zircon is a heavy mineral; therefore, it is easily concentrated by conventional heavy mineral separation methods (e.g., Morton et al., 2001). Thus, the petrographic, geochemical and isotope characteristics of zircons have been used for provenance studies (Morton., et al., 2001; Fedo et al., 2003; Yang et al., 2012). Physical petrographic characteristics, such as roundness, sphericity and grain fracturing, have been used to estimate transport type, distance from the source and energy capacity of the transport flow (Gärtner et al., 2013; Zoleikheai et al., 2016; Shaanan and Rosenbaum, 2018). Additionally, the morphology of the grains based on the typological classification diagram developed by Pupin (1980) has been used in palaeogeographic reconstructions (Loi and Dabard, 1997). Other studies have investigated the relationship of the internal texture of zircon to its growth stages and conditions within the magma reservoir (Vavra, 1990; Corfu et al., 2003). All these petrographic analyses have been complemented with detailed in situ grain analyses, including Hf and O isotopes (Wang et al., 2012; Zheng et al., 2021), trace elements (Xie et al., 2012) and combined dating, such as (U/Th)-He and U-Pb (Thomas, 2012; Yang et al., 2012; Shaanan and Rosenbaum, 2018; Riquelme et al., 2018).

These studies make zircon one of the most useful source indicator minerals in sedimentary successions.

Magmas with a high oxidation state (Fayalite-Magnetite-Quartz [FMQ] buffer +1 to +2; Richards 2015; Sun et al., 2017), high water content (≥ 4 wt % H_2O; Richards, 2003, 2011; Richards et al., 2012; Loucks, 2014; Loucks et al., 2020) and high degree of fractionation (Richards et al., 2001; Richards 2003, 2011) supply the necessary conditions to form porphyry copper deposits. Several studies have shown the application of zircons to ore genesis studies (e.g., Ballard et al., 2002; Muñoz et al., 2012; Shen et al., 2015; Dilles et al. 2015; Lu et al., 2016; Pizarro, 2019; Pizarro et al., 2020; Lee et al., 2021; Petrov et al., 2021; Nathwani et al., 2021). Zircon geochemical signatures can differentiate between porphyry Cu fertile and non-fertile intrusive bodies (Ballard et al., 2002; Dilles et al., 2015; Shen et al., 2015; Lu et al., 2016; Petrov et al., 2021). More recently, Pizarro et al. (2020) have used the PIZ concept to define a group of geochemical indicators tested in zircons collected from porphyry copper deposits worldwide that display common characteristics such as high Hf concentrations (>8,750 ppm), high Ce/Nd (>1), Eu/Eu* (>0.4), (10,000×Eu/Eu*)/Y (>1), (Ce/Nd)/Y (>0.01), intermediate Th/U (0.1–1) and low Dy/Yb (<0.3) ratios. In addition, these zircons show euhedral morphologies mainly characterised by prismatic forms of type {110} (Muñoz et al., 2012; Pizarro et al., 2020) and internal textures formed by zoned, weakly zoned or unzoned cores and strongly oscillatory zoned rims (Lu et al., 2016; Pizarro et al., 2020; Nathwani et al., 2023). Thus, geochemical signatures complemented by petrographic characteristics of zircons have been used as indicators of porphyry fertility. However, while zircons from igneous rock exposures have been studied, the detrital zircons have rarely been systematically tested in samples from the sedimentary record close to the copper porphyries (Lee et al., 2021), although this knowledge could increase success in greenfield exploration.

In this paper, we present the petrographic characteristics (microscopic observations and cathodoluminescence) and geochemical signatures (Electron Microprobe Analysis [EMPA] and Laser Ablation-Inductively Coupled Plasma-Mass Spectrometry [LA-ICP-MS]) of detrital zircons collected from late Cenozoic sediments from Centinela District in Northern Chile (Fig. 1). The Cenozoic stratigraphy is exposed in the open pit of the El Tesoro exotic-copper deposit and its surroundings. This location is within 2–4 km of several porphyry centres, including Llano, Esperanza and Mirador (Figs. 1, 2a). This study aims to validate PIZ as a tracer of the presence of buried porphyry copper deposits and confirm its use as a potential exploration tool for areas covered by sediments (e.g., gravel, sand, till).

2 Geological Setting

The Centinela District is located in the Antofagasta region (Northern Chile), ~40 km southwest of Calama city, at an elevation of about 2,300 m.a.s.l. (Fig. 1). The area includes several mid-late Eocene porphyry copper deposits (Mirador, Esperanza, Esperanza Sur, Llano, Encuentro, Penacho Blanco and Polo Sur), which belong to the ~800-km-long Chilean Upper Eocene-Lower Oligocene porphyry copper belt (Maksaev and Zentelli, 1999; Perelló et al., 2010; Mpodozis and Cornejo, 2012). The Centinela District also includes exotic copper deposits (El Tesoro and Tesoro NE) (Fig. 1 and 2).

The Centinela District is located at the western boundary of the Precordillera (Perelló et al., 2004, 2010) (Fig. 1). It is controlled by faults related to the Domeyko Fault System, a major zone of tectonic deformation stretching for >1000 km along the Precordillera (Maksaev and Zentelli, 1999; Mpodozis and Cornejo, 2012). The basement of the Centinela District comprises a wide variety of Late Palaeozoic to Early Cenozoic intrusive, volcanic, metamorphic and sedimentary rocks (Fig. 1c) originating from the Early Cretaceous through the Upper Eocene from semi-

continuous magmatic activity (e.g., Perelló et al., 2004; Mpodozis and Cornejo, 2012). At a regional scale, magmatic activity was focused mainly during the Middle Eocene-Early Oligocene (e.g., Mpodozis and Ramos, 1989; Scheuber and Reutter, 1992) and in the Centinela District, the porphyry copper deposits were emplaced near the surface between 45 and 39 Ma (Maksaev and Zentelli ,1999; Perelló et al., 2004; Mpodozis and Cornejo, 2012; Sanchez et al., 2018). Structurally controlled intramontane forearc basins developed in the Precordillera, mainly filled with gravels derived from the erosion of Eocene Precordilleran rocks (e.g., May et al., 1999; Riquelme et al., 2018). This sedimentary infill hosts several exotic copper deposits, such as Mina Sur in the Chuquicamata District or El Tesoro in the Centinela District. These deposits result from the exhumation and oxidation of copper mineralisation, and lateral transport and precipitation of the copper in the adjacent gravels (Münchmeyer, 1996; Sillitoe, 2005; Fernández-Mort et al., 2018).

The sedimentary record of the Centinela District comprises ca. 800 meter thick of coarse-grained alluvial facies continental deposits, with a few volcanic and tuff layers. Based on stratigraphic relationships, sedimentary facies and thicknesses, the following stratigraphic gravel units are recognised within the study area: Esperanza (middle-upper Eocene), Atravesados (upper Eocene-Oligocene), Tesoro (Oligocene-lower Miocene) and Arrieros (lower to middle Miocene) (Riquelme et al., 2018; Fernández-Mort et al., 2018). Ar/Ar dating and U/Pb detrital zircon data indicate the gravel units were deposited between the Middle Eocene and the Late Miocene (Riquelme et al., 2018). These units are partly covered by a thin layer of recent (<10 Ma) gravels (Pizarro et al., 2019). In the Centinela District, only El Tesoro (Tes), Arrieros (Arr) and Recent gravels host exotic copper mineralisation (Fig. 2c).

The Tesoro gravels include a ca. 240-m-thick deposit composed of three subunits: the lower (Tesoro I), middle (Tesoro II) and upper (Tesoro III) subunits (Fernández-Mort et al., 2018). The

Tesoro I (ca. 200-m-thick) subunit is composed of consolidated massive conglomerates and ungraded conglomerates, with sand and mud beds and minor intercalations of cross-bedded conglomerates and sandstones (Riquelme et al., 2018). The Tesoro II (ca. 70-m-thick) subunit is composed of consolidated cross-bedded and horizontally laminated conglomerates and sand beds, with minor intercalations of massive conglomerates, sandstones, siltstones, and sandy limestones. The Tesoro III gravels (ca. 90-m-thick) are formed by well-stratified conglomerates and minor ungraded conglomerates, sandstones, and siltstones. Provenance analyses (detrital zircons and clast composition) indicate that Tesoro II and Tesoro III sediments come from the rock units currently outcropping in the Centinela District. They were mainly derived from the erosion of the Upper Palaeozoic and Triassic basement rocks of the Sierra Limón Verde (granodiorites and granite), Upper Cretaceous rocks from the Quebrada Mala Formation (andesitic and dacitic tuff and volcanoclastic sandstones), Upper Cretaceous and Palaeocene intrusive bodies (porphyric rhyolites) and the late Eocene rocks of the Esperanza gravels (interbedded volcanic layers unit with conglomerates). Furthermore, the Tesoro II subunit contains a large population of clasts and zircons derived from the erosion of nearby porphyry copper deposits (propylitic and phyllic altered clasts), and this subunit hosts the lower exotic-Cu ore body at El Tesoro (Fig. 2c).

The Arrieros gravels (Arr) is about 100 metres thick and composed of poorly consolidated horizontally laminated conglomerates with minor intercalations of massive sands and silts. Similarly, to the Tesoro II and III gravels, both clast lithologies and detrital zircon populations indicate that almost all of the rock units outcropping in the Centinela District were already exposed and eroded at the time the Arrieros gravels were deposited. The conglomerate clasts are a distinctive population of the Arrieros gravels that can only have resulted from the erosion of the underlying gravel deposits. Another distinctive clast lithology of this unit comes from the Jurassic

to Lower Cretaceous Caracoles Group (limestones and calcareous siltstone). Also, the Arrieros gravels contain a large population of zircons derived from the erosion of nearby porphyry copper deposits, and this unit hosts the upper exotic-Cu ore body in the El Tesoro pit (Fig. 2c).

The Recent gravels correspond to the uppermost part of the gravel sequence and are composed of semi-consolidated massive conglomerates and ungraded, mainly coarse-grained conglomerates deposited over a large part of the study area, albeit with a typical thickness of less than 5 m. The composition of the clasts is similar to that of the Arrieros gravels, and they were deposited post-10 Ma (Pizarro et al., 2019). This unit contains traces of exotic copper mineralisation (Fig. 2c).

3 Sampling and Methodologies

Seven samples of approximately 7 kg each were selected for zircon petrographic and geochemical analysis. These samples were taken from the sedimentary rocks of the Centinela District and represent gravel units with exotic copper mineralisation and unmineralised gravels from the El Tesoro exotic copper deposit pit and its surroundings (Fig. 2b). In the Tesoro II gravels, the Ts01 sample was taken from the gravel horizons located below the lower exotic Cu body, whereas the Ts02 sample was taken directly from the lower exotic Cu body. Two samples (Ts03 and Ts04) were taken from the unmineralised Tesoro III gravels. Sample Ts05 was taken from the Arrieros gravels in the upper exotic Cu body, whereas Ts06 was taken from a palaeochannel filled with gravels with traces of exotic Cu mineralisation located outside the pit. The Ts07 sample comes from recent alluvial gravels just above Ts06.

The seven samples were sieved through a 0.5-mm mesh, and then the zircons were separated by conventional separation procedures, including a vibrating water table, heavy liquids (Diiodomethane, 3.31 g/cm^3) and magnetic separation (inclination 20° and >1.2 Amps). This

procedure was carried out at the Mineral Deposit Research Unit (MDRU) of the University of British Columbia, Canada. Representative zircons from all gravel units were hand-picked, mounted in epoxy resin discs, and polished to approximately half-grain thickness. In this study, about 15 zircons per sample were analysed based on the number of grains used in similar studies (e.g., Muñoz et al., 2012; Shen et al., 2015; Pizarro et al., 2020). The number of analyses required to produce a statistical description of detrital zircon in a regional setting for provenance studies remains a topic of debate (e.g., Andersen, 2005). Vermeesch (2004) has suggested that 117 grains should be dated to be 95% confident that no fraction equal to or less than 0.05 of the population has been overlooked. However, a recent study by Lee et al., (2021) has proposed that 14 to 31 zircon crystals per sediment sample are sufficient to define a broad regional pattern in geochemical values linked to the fertility potential of a porphyry ore deposit.

A transmitted light microscope was used to study the petrographic characteristics of the zircon grains, such as morphology and internal structure (Fig. 3a). These studies were complemented with cathodoluminescence (CL) images obtained through Electron Microprobe Analysis (EMPA) using a Cameca SX-Five FE mounted on a Scanning Electron Microscopes (SEM) at the Centre de Microcaractérisation Raimond Castaing (CMRC), CNRS, Toulouse, France (Fig 3b). Petrographic studies of the zircon grains showed that some grains have small inclusions (<30 μm), and the areas with inclusions were avoided for analysis.

The concentrations of major, minor and trace elements in the zircons were measured in situ using EMPA with a Cameca SX-Five at CMRC. The analyses were done in the wavelength dispersion mode with the following operating conditions: excitation voltage, 15 kV; beam current, 20 nA; peak count time for the elements, 15 s (peak count time for background, 5 s and peak count time for data collection, 10 s); and spot diameter, 4 μm. Data reduction was done using the 'PAP'

$\phi(\rho Z)$ method (Pouchou and Pichoir 1985). For the elements considered, the following standards, X-ray lines and crystals were used: corundum (Al), wollastonite (SI, Ca), hematite (Fe), YPO_4 (Y), reference zircon (Zr), $CePO_4$ (Ce), $DyPO_4$ (Dy); UO_2 (U), synthetic graftonite (Pb), ThO_2 (Th), HfZr (Hf) and graphite (P). The detection limits for zircon used by this program were: Al. (260 ppm), Si (320 ppm), Ca (920 ppm), Fe (950 ppm), Y (850 ppm), Zr (1,450 ppm), Ce (2,200 ppm), Gd (5,000 ppm), Dy (2,600 ppm), U (1,200 ppm), Pb (2,300 ppm), Th (3,500 ppm) and Hf (1,200 ppm) (see Appendix A for details).

The geochemical signatures of the zircons were measured by laser ablation-inductively coupled plasma-mass spectrometry (LA-ICP-MS) using a NewWave Research UP213 laser coupled to an Agilent 7500 ICP-MS instrument at the Géosciences Environnement Toulouse laboratory (GET), Observatoire Midi-Pyrénées, Toulouse, France. The counting time for each analysis was 180 s (60 s on a gas blank to establish the background and 120 s for data collection), the diameter of the laser beam was 34 μm, and the frequency was 7 Hz with 4 J/cm^2 of laser fluence. A maximum of 10 unknowns were bracketed by the measurement of two external standards, which corresponded to NIST SRM 610 (primary) and NIST SRM 612 (secondary) glass. The data reduction was performed with Glitter software (Griffin et al., 2008) using the ^{29}Si content determined by EMPA as an internal standard.

During the data reduction, a careful check of the multi-element mass spectra allowed the elimination of any possible impurities that may have been encountered across the depth profile of each laser-ablated area by assessing the ^{29}Si profile. The first filter to determine any contamination from inclusions or other phases was the Ca content because the latter is low in zircon (e.g., Shen et al., 2015). Next, spot analyses affected by contamination related to small mineral inclusions or cracks within zircons were discarded by applying filtering mechanisms, specifically, the ‘clean

zircon' standard (Zou et al., 2019; La <0.1 ppm) and the LREE-I index (Bell et al., 2016; LREE-I (Dy/Nd + Dy/Sm) <30; Appendix A). A total of 182 spots on 99 zircon grains were analysed; once the filtering mechanisms were applied, 58 spots and 21 zircon grains were rejected because of contamination. In each zircon, two ablations (spots) were analysed, one at the core and one at the rim, to check for significant geochemical variations between these areas in individual grains. The detection limits for each element are in the range of 10 to 60 ppb, except for Sc and V (100 ppb), Ti (2 ppm), and Ni and Cr (0.7 ppm). If the elemental concentrations in the LA-ICP-MS data were below the detection limits, values of half a detection limit were used to display the data graphically.

4 Results

4.1 Petrographic characteristics of detrital zircon

The morphological characteristic of detrital zircons can provide valuable information about the provenance and palaeo-drainage in sedimentary basins (Gärtner et al., 2013; Zoleikheai et al., 2016). The morphological classification in this study was performed on 99 zircon grains based on their petrographic characteristics (Figs. 3, 4; Table 1). The zircon grains found in the sedimentary record are typically non-fractured. The Tesoro III, Arrieros and Recent gravels have more than 60% non-fractured zircon grains, while in the Tesoro II gravels, the concentration of non-fractured grains decreases by 43% (Fig. 4; Table 1), mostly near the bottom of the stratigraphic sequence.

The length of the zircon along the c-axis varies between 90 and 450 µm and the width varies between 50 and 150 µm (Appendix B), irrespective of sedimentary unit (Fig. 3). To quantify and compare the morphological characteristics of the zircon grains, the roundness and sphericity of all analysed grains were recorded following the methodology proposed by Shaanan and Rosenbaum (2018). The roundness was ranked on a relative scale of 1–5, representing anhedral to prismatic euhedral morphology, respectively (R1 to R5, Appendix C). The scale is normalised in percentage

with a value of 100%, indicating fully rounded or abraded grains. The aspect ratio or sphericity was calculated for whole grains only (not in fractured grains) as the ratio of the apparent elongated axis of a grain divided by the perpendicular axis (i.e., length/width) (Appendix C). Thus, grains having an aspect ratio <2 were assigned to S1, those between 2 and 3 to S2 and those >3 to S3 (Fig. 4; Table 1).

In the Tesoro gravels, the roundness of zircon is mainly moderate (R3), between subrounded and subangular (Fig. 4; Table 1). The Recent gravels and the top of the Arrieros gravels (Ts06) present a greater number of rounded zircons (R1-R2), ca 50% of the grains (Fig 4; Table 1; Appendix B), whereas the bottom of Arrieros (Ts05), Tesoro II and Tesoro III gravels have a greater number of moderate (R3) and non-rounded zircons (R4-R5) (Fig. 4; Table 1; Appendix B). The aspect ratio of the zircons varies between 1 and 5 (Appendix B) and is mainly dominated by a greater number of zircons with regular shapes (S2), i.e., zircons with an aspect ratio between 2 and 3 (Fig. 4; Table 1; Appendix B). A significant number of elongated grains is only present in the Tesoro III gravels (Fig. 4; Table 1; Appendix B), while the top of Arrieros gravels (Ts06) is the only place of the stratigraphic column where square zircon grains are observed (S1).

The studied zircons show external euhedral to anhedral morphologies. For the morphological characterisation of the zircons, we used 72 not fractured or slightly fractured grains. They were classified using the typological classification developed by Pupin (1980), in which zircon crystals are classified according to the relative development of the prismatic forms {100} vs. {110} and pyramidal forms {211} vs. {101}. The morphologies of the detrital zircons typically show prismatic forms of type {110}. Only in the Arrieros gravels can a significant number of prismatic forms of type {100} be observed. They occur in an abundance greater than 35% (Fig. 3;

Table 1). Zircons with pyramidal forms of types {101} and {211}, were found throughout the stratigraphic section (Fig. 3; Table 1).

With respect to the internal structures, the zircon grains present unzoned cores and strongly oscillatory zoned rims, whereas grains with oscillatory zoning from core to rim are scarce (Fig. 3). Other textures, such as internal structures parallel to the prisms or without a clear pattern of growth, were observed (Fig. 3). In some grains, the internal textures are interrupted by cracks, reabsorption textures or inherited cores (Fig. 3). In addition, melt inclusions are present in a large number of grains (Fig. 3). The mineral inclusions in zircon correspond mainly to apatite and opaque minerals. The internal structures from the studied zircons do not have a clear relationship to any particular part of the stratigraphy.

4.2 Geochemical signatures of detrital zircon

4.2.1 Rare earth element patterns

The abundance of the rare earth elements (REE) in zircon grains is normalised to the chondrite values from McDonough and Sun (1995). The results show that the REE patterns of the detrital zircons from the different sedimentary units studied are similar. They display low light REE (LREE) and elevated heavy REE (HREE) contents with distinctive positive Ce and negative Eu anomalies (Fig. 5). These patterns are similar to those from zircons coming from porphyry copper deposits and arc magma intrusions (e.g., Ballard et al., 2002; Shen et al., 2015; Lu et al., 2016; Pizarro et al., 2020; Petrov et al., 2021).

4.2.2 Geochemical signatures

Variation in the geochemical and isotopic signatures measured in zircons has been used as a powerful tool to differentiate between different sources (e.g., Belousova et al., 2002; Ballard et

al., 2002; Lu et al., 2016; Lee et al., 2017;). High Hf (>8.750) concentration and high Ce/Nd (>1), Eu/Eu* (>0.4), 10,000×(Eu/Eu *)/Y (>1) and (Ce/Nd)/Y (>0.01) ratios, and low Dy/Yb (<0.3) and intermediate Th/U (0.1–1) ratios have been linked to zircons originating from porphyry copper deposits worldwide (Ballard et al., 2002; Muñoz et al., 2012; Dilles et al., 2015; Shen et al., 2015; Lu et al., 2016; Pizarro et al., 2020; Lee et al., 2021; Petrov et al., 2021; Nathwani et al., 2021). In addition, zircons coming from porphyry copper deposits have lower Ti (<9 ppm) compositions (e.g., Quellaveco District, Southern Peru; Nathwani et al., 2021) and high Ce/Ce* values as observed in porphyries worldwide (e.g., Ballard et al., 2002; Shen et al., 2015). Nevolko et al. (2021) have reported Ce/Ce* values >750 in zircons from the Bystrinsky and Shakhtama porphyry Cu-Mo-Au deposits of Eastern Transbaikalia, Russia. All these values have been linked to evolved, oxidised, water-rich, and fractionated magmas thought to form porphyry copper deposits (e.g., Ballard et al., 2002; Dilles et al., 2015; Lu et al., 2016). Thus, this work focuses on these geochemical signatures for the detrital zircon of the Centinela District to trace the presence of porphyry copper bodies adjacent to the sedimentary record.

The measured zircon grains present significant geochemical variety (Table 2; Appendix A), which can be linked to the diversity of rocks outcropping in the source area (Perelló et al., 2010; Riquelme et al., 2018). Figure 6 shows the relationship between the (Ce/Nd)/Y and Eu/Eu* ratios. The (Ce/Nd)/Y ratio varies between 0.001 and 0.394, with an average value of 0.022 (Table 2). The Eu/Eu* ratio varies between 0.09 and 0.85, with an average value of 0.48 (Table 2). There is no overall correlation between (Ce/Nd)/Y and Eu/Eu* ratios, but a large number of zircons have (Ce/Nd)/Y values greater than 0.01 and Eu/Eu* values higher than 0.4 (Fig. 6). Over 95% of the analysed zircon grains have Ce/Nd >1, (10,000×Eu/Eu *)/Y >1, Dy/Yb <0.3 and Th/U between 0.1 and 1, as well as Hf concentration that vary between 5,978 and 14,462 ppm with an average

value of 9,964 ppm (Table 2). The Ti concentrations range between 1.42 and 50.16 ppm, with an average value of 9.16 ppm (Table 2). The Ce/Ce* values were calculated from the spreadsheet shared in Nevolko et al. (2021) and vary between 20 and 17,078, averaging 709 (Table 1). Therefore, the geochemical composition of some zircons in the gravels overlaps with the profiles typically of porphyry copper deposits.

5 Discussion

5.1 Petrographic and geochemical characteristics of PIZs

The detrital zircons from the sedimentary record of the Centinela District show important geochemical and morphological differences. All sedimentary units contain several zircon grains with Hf concentrations >8,750 (ppm) and (Ce/Nd)/Y >0.01 and Eu/Eu* >0.4 values. Additionally, a large percentage of the studied zircons have Ce/Nd >1, (10,000×Eu/Eu *)/Y >1, Dy/Yb <0.3 and Th/U between 0.1 and 1 (Table 2). No specific geochemical trend between stratigraphic units can be discerned (Fig. 6). The significant scatter in the zircon geochemistry is attributed to the great diversity of potential source rocks in the area, which were already exposed and eroded at the time of gravel deposition (Perelló et al., 2004, 2010; Riquelme et al., 2018). To validate zircon as a tracer of buried copper porphyries in the adjacent sedimentary record and check its use as a potential exploration tool, we used the PIZ (Porphyry Indicator Zircon) concept (Pizarro et al., 2020), which is a group of geochemical indicators for zircons. A PIZ needs to comply with each of the following geochemical criteria: Hf >8,750 (ppm), Ce/Nd >1, Eu/Eu* >0.4, (Ce/Nd)/Y >0.01, 10,000×(Eu/Eu *)/Y >1, Dy/Yb <0.3 and $0.1 < Th/U < 1$. These values have been linked to magmas with a high oxidation state (FMQ + 1 to + 2; e.g., Ballard et al., 2002; Shen et al., 2015; Dilles et al., 2015), a high water content (≥4 wt% H_2O; e.g., Lu et al., 2016) and a high degree of fractionation (e.g., Muñoz et al., 2012; Dilles et al., 2015; Lu et al., 2016; Kirkland et al., 2015),

which corresponds to the conditions necessary to form a porphyry copper deposit (Sillitoe 2010; Richards 2003, 2015; Seedorff et al., 2005; Chambefort et al., 2008). However, these geochemical signatures have also been associated with enrichment in the residual magma, either as a result of plagioclase suppression (e.g., Nathwani et al., 2020) or due to the co-crystallization of other minerals, such as titanite, apatite, and/or amphibole (e.g., Loader et al., 2022; Matthews et al., 2023).

Once the PIZ filter is applied to detrital zircons, 36% of the detrital zircons found in the sedimentary record of the Centinela District correspond to PIZs, and their concentration varies throughout the stratigraphic sequence. The highest PIZ concentrations are found in Tesoro II gravels at 56%, whereas Tesoro III gravels have the lowest concentration, 15% (Fig. 7; Table 2). The median PIZ concentrations in the Arrieros and Recent gravels are 32% and 28%, respectively (Fig. 7; Table 2). The Hf concentration and (Ce/Nd)/Y and Eu/Eu* ratios of the PIZs strongly overlap with the compositional fields for zircons from the copper porphyry deposits of Esperanza and Mirador (Fig. 7), located 2 and 4 km respectively from the El Tesoro pit (Fig. 2a). However, the Dy/Yb and Th/U ratios of the PIZs do not overlap with compositional fields of the porphyry zircons (Fig. 7). The Dy/Yb and Th/U ratios are lower than those documented in the zircons from Mirador and Esperanza porphyries. The lower Dy/Yb ratios of the PIZs present in the gravels may result from their formation within hydrous magmas characterized by a higher amphibole content. Amphibole tends to preferentially incorporate middle rare earth elements (REE) over heavy REE (Davidson et al., 2007), leading to a decrease in Dy/Yb ratio values within the residual magma and consequently in the zircons themselves (Davidson et al., 2007; Richards and Kerrich, 2007; Lu et al., 2015). The lower Th/U values found in the PIZs within the gravels could be attributed to their formation within a less fractionated magma. While both thorium (Th) and uranium (U) are

primarily incompatible with major rock-forming minerals, they are compatible with zircon (e.g., Bea, 1996; Hoskin et al., 2000; Hanchar and van Westrenen, 2007). However, Th is less compatible compared to U, leading to its retention in the residual melt (Kirkland et al., 2015) Thus, PIZs collected from the gravels may have crystallized earlier than those from the Mirador and Esperanza porphyries within the same magmatic chamber, during a period when the magma was less evolved, or they might have eroded from an as-yet-undiscovered porphyry source.

In order to check the use of zircon as a tracer of the presence of buried copper porphyries in adjacent sediments, Lee et al., (2021) have identified zircon with Eu/Eu* >0.4 from surface till samples adjacent to and 9 km down-ice from the Highland Valley Porphyry District (British Columbia, Canada). However, they have only used this chemical indicator to differentiate between detrital zircons coming from porphyry Cu fertile and non-mineralised intrusive bodies. In the sediments of Centinela District, the percentage of detrital zircon with Eu/Eu* >0.4 is 61%. According to the methodology proposed by Lee et al. (2021), the percentage of grains that could be linked to a copper porphyry deposit would increase notably. Something similar happens when we use any other geochemical indicator individually; for example, the percentage of detrital zircons with (Ce/Nd)/Y >0.01 is 65%, and Hf concentrations >8,750 (ppm) is 69% (Figs. 7, 8), while zircons with another geochemical indicator are greater than 90%. Thus, the implementation of PIZ criteria allows us to discard detrital zircons coming from non-mineralised intrusive bodies, which may have been formed from magmas with a high oxidation state, high water content or high degree of fractionation, whose zircons can also have Eu/Eu* >0.4, (Ce/Nd)/Y >0.01,or Hf concentrations >8,750, presenting only some of these chemical indicators (Ballard et al., 2002; Dilles et al., 2015; Lu et al., 2016). In addition, some magmas are evolved (i.e., high SiO_2) but fractionated a plagioclase-dominated assemblage rather than an amphibole-dominated one, reflected by a Dy/Yb

>0.3 in zircons (Lu et al., 2016), which occurs in relatively dry magmas (Davidson et al., 2007; Richards and Kerrich, 2007). Also, the gravels may contain zircons of metamorphic origin or with evidence of recrystallisation processes, which can have Eu/Eu* >0.4 but Th/U <0.1 (Rubatto 2002).

Additionally, 100% of the PIZs found in gravel deposits have Ti concentrations <9 ppm (Fig. 8; Table 1), reinforcing the use of this geochemical indicator as a probable fertility tracer, as proposed by Nathwani et al., (2021). Also, 92% and 81% of the zircons from Mirador and Esperanza porphyries, respectively, have Ti concentrations of less than 9 ppm (Fig. 8). This low Ti concentration in zircons is related to low-temperature magmas (<800°C) (Nathwani et al., 2021). Pizarro et al., (2020) have estimated a temperature range between 605 and 730°C for nearby porphyries, including Mirador and Esperanza. These temperatures were calculated using the Ti-in-zircon thermometer, assuming an activity in the melt of $aSiO_2 = 1$ and $aTiO_2 = 0.7$ (Ferry and Watson, 2007). Thus, this Ti concentration (<9 ppm) can be included in the PIZ criteria. On the other hand, some authors have linked the high Ce/Ce* values recorded in zircons to the high oxidation state of the magma (e.g. Ballard et al., 2002; Shen et al., 2015), a critical factor for the formation of porphyry deposits (e.g., Richards, 2003; Loucks, 2014). Nevolko et al., (2021) have recorded Ce/Ce* >750 in zircons from the Bystrinsky and Shakhtama porphyry Cu-Mo-Au deposits of Eastern Transbaikalia, Russia. In our study, the percentage of PIZs that present Ce/Ce* >750 is relatively low; only 20% of the PIZs found in the gravel deposits meet this condition (Fig 8; Table 1). Furthermore, only 23% and 44% of the zircons from the Mirador and Esperanza porphyries, respectively, have Ce/Ce* >750 (Fig. 8). Thus, the critical threshold of Ce/Ce* (>750) proposed by Nevolko et al. (2021) is not useful in this study. Although PIZs tend to have higher Ce/Ce* than the zircon no porphyry indicator found in gravel deposits, and they present the same values as the zircons from Mirador and Esperanza porphyries. All PIZs from the sedimentary

record have Ce/Ce* >100, while 87% and 98% of the zircons from Mirador and Esperanza, respectively, comply with this condition (Fig. 8; Table 1). However, this geochemical indicator must be used as a fertility tracer with caution because a recent study by Loader et al. (2022) has demonstrated that increases in the magnitude of the Ce anomaly may occur as a natural consequence of cooling magmas at constant melt redox conditions and that this effect is magnified by increasing the melt Ce/Nd ratio, which can be driven by the co-crystallisation of amphibole, apatite and especially titanite.

The petrographic characteristics do not show a clear correlation with PIZ concentration, except for the external morphology of the grain, which is controlled by endogenous factors, such as temperature and polymerisation of the melt as a result of composition (Pupin, 1980; Corfu et al., 2003; Rezeau et al., 2019). Zircons coming from copper porphyries show euhedral morphologies characterised by prismatic forms of type {110} and pyramidal forms mainly of types {101} and {211} (Muñoz et al., 2012; Pizarro et al., 2020). This external morphology characterisation has been used in some studies as the petrogenetic signature of the source rocks in which they crystallised (Loi and Dabard, 1997; Belousova et al., 2005). In our data, we observe a relationship between PIZs and the external morphology of the detrital zircons. Around 85% of PIZs have euhedral external morphologies characterised by the exclusive development of prismatic forms of type {110} (Table 2; Appendix B). This crystallographic form is typical of magmas that crystallised at low temperatures (Pupin 1980, Bolousova et al., 2005; Muñoz et al., 2012). Also, 100% of the zircons from Esperanza, Mirador, Escondida and Chuquicamata porphyry copper deposits have euhedral morphologies characterised by prismatic forms of type {110} (Pizarro et al., 2020). PIZs with grain morphologies characterised by prismatic forms of type {100} are only found in the Arrieros gravels.

There is no direct relationship between the PIZs and petrographic characteristics controlled by exogenous factors, such as erosion and transport. However, a relationship between the roundness and fracturing of zircons with a stratigraphic unit can be observed (Fig. 4). It is widely accepted that roundness results from the abrasion of grain margins caused by long-term transportation or reworking by the transporting medium (e.g., Russell, 1955). In turn, the fracturing of zircons is controlled by the effective energy during the transport process, which is directly related to high- or low-energy transport (Gärtner et al., 2013). In the sedimentary record of the Centinela District, the roundness of the zircons is mainly moderate, giving subrounded to subangular (R3) grains; however, the Recent and Arrieros gravels are the only units that have a high concentration of rounded zircons (R1- R2). They contain 50% and >38% rounded zircons, respectively, whereas the Tesoro III and Tesoro II gravels only contain around 20% (Fig. 4; Table 1). From this, we can infer that the Recent and Arrieros gravels were deposited farther from their source than the Tesoro gravels. This increasing distance may be due to the retreat of the initial topographic front (Riquelme et al., 2018) and/or to the reworking of previously deposited zircons. In the Tesoro III gravels, 57% of zircon grains are fractured, whereas for the Tesoro II, Arrieros and Recent gravels, the fractured grain concentration is less than 40% (Fig. 4; Table 1). All studied units were deposited in an arid continental environment dominated by alluvial fans, that is, by a high-energy flow (Fernández-Mort et al., 2018; Riquelme et al., 2018). Thus, we can infer that the Tesoro III gravels were transported by an alluvial transport with higher energy than the Tesoro II, Arrieros and Recent gravels. A more complete interpretation of the paleogeographic evolution of the study area would require the study of a greater number of detrital zircons.

5.2 PIZ in the sedimentary record of Centinela District

The highest PIZ concentrations in the sedimentary record of the Centinela District coincide with gravel horizons located close to the base that hosts the lower exotic Cu body with 61% and 50% PIZ concentrations for Ts01 and Ts02 samples, respectively (Fig. 9). These horizons also contain a large number of clasts from the erosion of the propylitic and phyllic hydrothermal alteration zones of the copper porphyries (Riquelme et al., 2018; Fernández-Mort et al., 2017). In this section of the sedimentary record, Riquelme et al. (2018) have documented an important population of detrital zircons, dated by LA-ICP-MS, with ages ranging between 39 and 46 Ma with a peak at 42 Ma (median calculated from 76 grains). These ages coincide with the U/Pb ages of zircons from the copper porphyry deposits in the area, including the nearby Esperanza (41.3 ± 0.3 Ma) and Mirador (40.6 ± 1.1 and 41.6 ± 2.4) porphyries (Perelló et al., 2004; Pizarro et al., 2020). Fernández-Mort et al. (2017) have shown that the lower exotic-Cu ore body was formed by the precipitation of oxidised copper minerals within permeable and unconsolidated gravel horizons from laterally surface-transported Cu-bearing aqueous solutions from copper porphyry. Therefore, the PIZs found in these horizons most probably come from porphyry copper deposits already exposed and eroded at the time of the gravel deposition.

The lowest PIZ concentrations are found in the Tesoro III gravels: 13% and 18% for Ts03 and Ts04 samples, respectively, coming from horizons without exotic-Cu mineralisation (Fig. 9). This low PIZ concentration also coincides with a lower concentration of clasts of hydrothermal origin from the erosion of porphyries and with detrital zircons of mainly Palaeozoic and Late Cretaceous to Palaeocene ages (Riquelme et al., 2018). This suggests a change in the source of the sediments or a reconfiguration of the drainage network during the deposition of these gravels.

In the Arrieros gravels, the PIZ concentration tends to increase: 38% and 29% for Ts05 and Ts06 samples, respectively, compared to the Tesoro III gravels (Fig. 9). This increase is because

these samples were taken in horizons hosting the upper exotic-Cu ore body of El Tesoro and from a paleochannel showing traces of Cu mineralisation, respectively. In the Arrieros horizons, the concentration of hydrothermal clasts tends to decrease compared with the Tesoro II gravels, and these horizons host a large population of detrital zircons that present ages ranging between 43 Ma and 36 Ma with a peak at 39 Ma (median calculated from 33 grains; Riquelme et al., 2018). The upper exotic-Cu ore body was also formed by the precipitation of oxidised copper minerals from Cu-bearing aqueous solutions. However, the presence of reworked clasts of chrysocolla and conglomerate clasts in this ore body also suggests that it could have been partly enriched by the physical erosion of the upstream part of the lower exotic-Cu ore body (Fernández-Mort et al., 2017). Thus, the PIZs found in these gravels can originate from the erosion of the surrounding porphyries and/or a previously formed exotic-Cu ore body, perhaps the lower exotic-Cu body of El Tesoro. The Arrieros graves horizons have a high concentration of rounded zircons, which indicates that they were transported for a long time or reworked, strengthening the interpretation of Fernández-Mort et al. (2017) regarding the origin of the lower exotic-Cu ore body.

In the Recent gravels, the PIZ concentration is 28%, which is very similar to the upper horizon of the Arrieros gravels (Fig. 9). This relatively high concentration is because the sample was taken just above a paleochannel that showed traces of Cu mineralisation. As shown by Lee et al. (2021) in till sediments in British Columbia, the samples taken from the sediment surface can contain an important number of zircons with a metallogenic fertility signature.

Approximately 64% of the detrital zircons found within the gravel units do not meet the PIZs criteria. They likely come from the diverse range of rock types present in the region, which had already been exposed and eroded at the time of gravel deposition. Riquelme et al. (2018) identified three other large detrital zircon populations in the Tesoro and Arrieros gravels:

Carboniferous-Permian (266–344 Ma), Late Cretaceous (68–74 Ma), and Palaeocene (57–63 Ma). These minerals were probably eroded from the volcanic and intrusive basement (Sierra Limón Verde - Sierra Agua Dulce), sedimentary and volcanic succession (Quebrada Mala Formation) and epizonal intrusions of acid composition, respectively. Consequently, these rocks represent alternative potential sources for the zircons no porphyry indicator observed throughout the sedimentary record.

Therefore, detrital zircons with the following geochemical values: Hf >8,750 (ppm), Ce/Nd >1, Eu/Eu* >0.4, 10,000×(Eu/Eu *)/Y >1, (Ce/Nd)/Y >0.01, Dy/Yb <0.3 and 0.1 < Th/U < 1 and with euhedral morphologies characterised by prismatic forms of type {110} can be used as a tracer of the presence of porphyry copper deposits in the adjacent sedimentary record. The gravel horizons with exotic-Cu mineralisation coincide with the highest concentration of PIZs, while the gravel horizons without exotic-Cu mineralisation exhibit the lowest concentration of PIZs. Additionally, a high concentration of PIZs does not always coincide with a high occurrence of clasts of hydrothermal origin, as observed in the Arrieros gravels; in this sedimentary environment, the clasts do not always resist transport and weathering, while zircons only suffer minor physical changes. In contrast, the use of detrital zircon age as the sole tracer for the presence of copper porphyries in sediments may lack efficiency because the age range of the detrital zircon population that could come from the erosion of porphyry copper might be wide (7 Ma here) and prevent the identification of specific episodes of mineralisation.

5.3 Exploration implications

The discoveries of economically viable porphyry copper deposits have decreased over time (Kelley et al., 2011). Most of the exposed copper porphyries on the surface have already been discovered, and exploration of those covered by sediments is a great challenge. Conventional

exploration methods, such as geophysical, reserve circulation (RC) and diamond drill hole (DDH), have high economic costs. In this competitive context, efficient, lower-cost alternative exploration methods are required. This research is a proof of concept that geochemistry and petrographic characteristics of detrital zircon can be used as indicators of the presence of copper porphyries in the adjacent sedimentary record. The PIZ approach has shown its efficiency in two important metallogenic provinces as a good indicator of porphyry copper deposits: (1) in alluvial gravel cover in the Atacama Desert, Chile (this work) and (2) in glacial till cover in British Columbia, Canada (Lee et al., 2021). Thus, this mineral can be used as an exploration tool in uncharted territories where there are no clasts with hydrothermal alteration (fragile to mechanical transport) or in the presence of copper of supergene origin (susceptible to environmental conditions). Therefore, investigations of the geochemical and petrographic characteristics of zircon in sediments that may cover and hide ore deposits should be developed and can help vectorise and limit exploration targets while reducing costs and making conventional exploration methods more effective.

Testing this methodology in different sedimentary environments and observing zircon behaviour, such as the dispersion in alluvial fans or the distance travelled in a fluvial or glacial system, remains to be done. It would also be useful to complement the use of zircon with other resistant minerals, such as apatite (Bouzari et al., 2016; Pan et al., 2016; Chen et al., 2021), rutile (Scott 2005; Rabbia et al., 2009), garnet (Russell et al., 1999), titanite (Nakada 1991; Piccoli et al., 2000), magnetite (Canil et al., 2016; Nadoll et al., 2015), tourmaline (Baksheev et al., 2012), epidote (Cooke et al., 2014b; Cooke et al., 2020) and chlorite (Wilkinson et al., 2015; Neal et al., 2018; Ahmed et al., 2020). However, except for magnetite (Pisiak et al., 2017), their use has not been tested in sedimentary records. Hence, the petrographic and geochemical characteristics of

different minerals resistant to weathering and transport present a fruitful area for future research focused on the search for new exploration targets.

6 Conclusions

The geochemical and petrographic characteristics of detrital zircons collected from the late Cenozoic sedimentary record from the Centinela District in Northern Chile were used to validate zircon as a possible tracer of the presence of porphyry copper deposits. The conclusions can be summarised as follows:

- In total, 36% of the detrital zircons found in the sedimentary record of the Centinela District correspond to porphyry indicator zircons (PIZ) and have a similar geochemical signature and petrographic characteristics as the zircons from the Mirador and Esperanza porphyry copper deposits, located 2 and 4 km from the sampling area, respectively.
- The PIZs can be used as a tracer of porphyry copper deposits in the sedimentary record because the highest PIZ concentrations coincide with the gravel horizons that host the upper and lower exotic copper bodies of El Tesoro. Also, these horizons have clasts related to the erosion of the hydrothermal alteration zones of the copper porphyries and an important population of zircons with ages that coincide with the age of mineralisation in the Centinela District.
- Also, PIZs can be used as a powerful exploration tool in the search for buried porphyry copper deposits under a sedimentary cover, limiting the exploration target size, reducing costs and making conventional exploration methods more effective.

Figures and Figure Captions

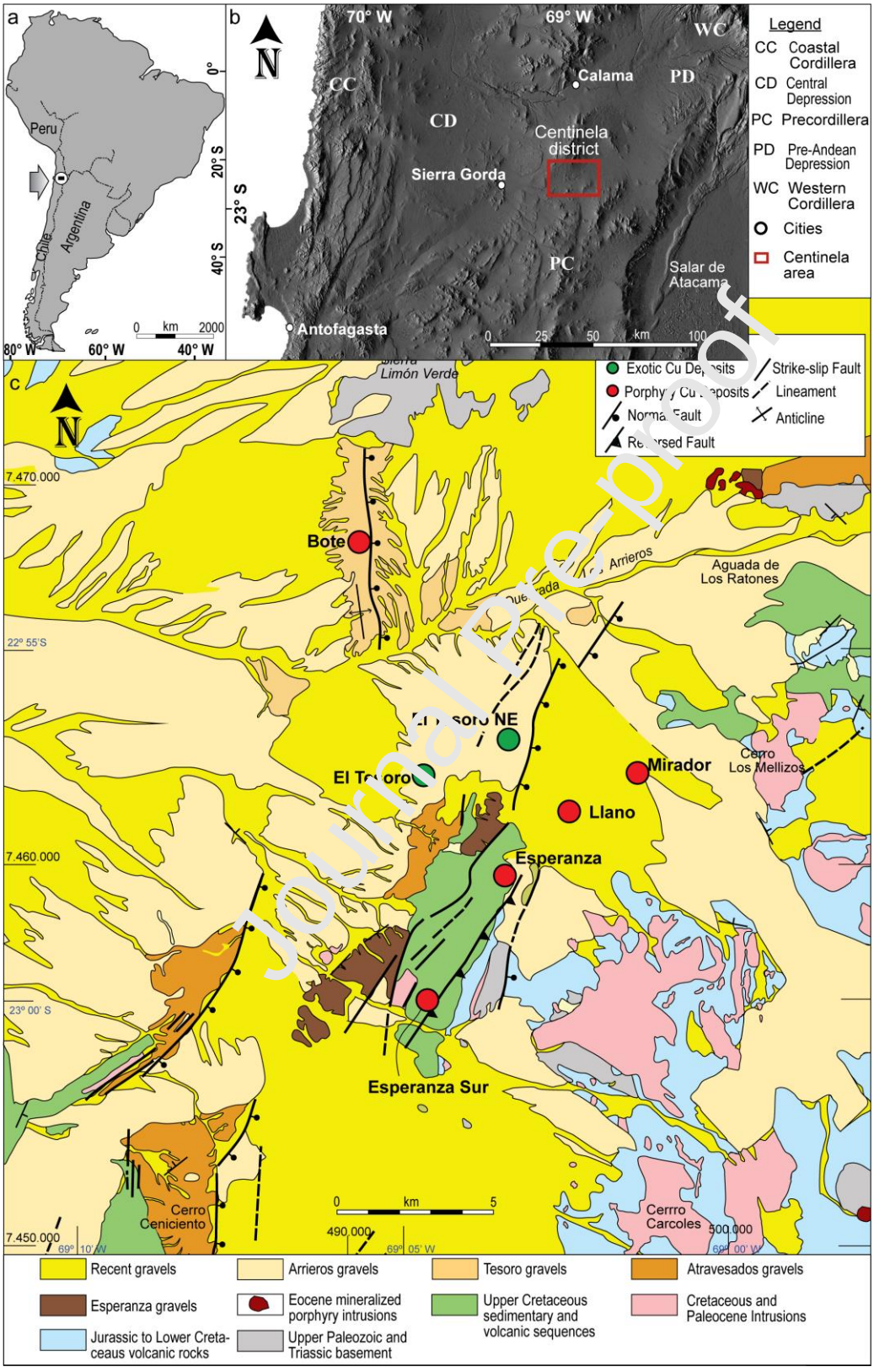

Fig. 1. Location and geology of Centinela District. **a** Map of South America. **b** Physiographic units of the Atacama Desert in the Antofagasta Region and location of Centinela District. **c** Geological map focused on the mid-Eocene to Miocene gravel units in the Centinela District (Modified from Pizarro et al., 2019)

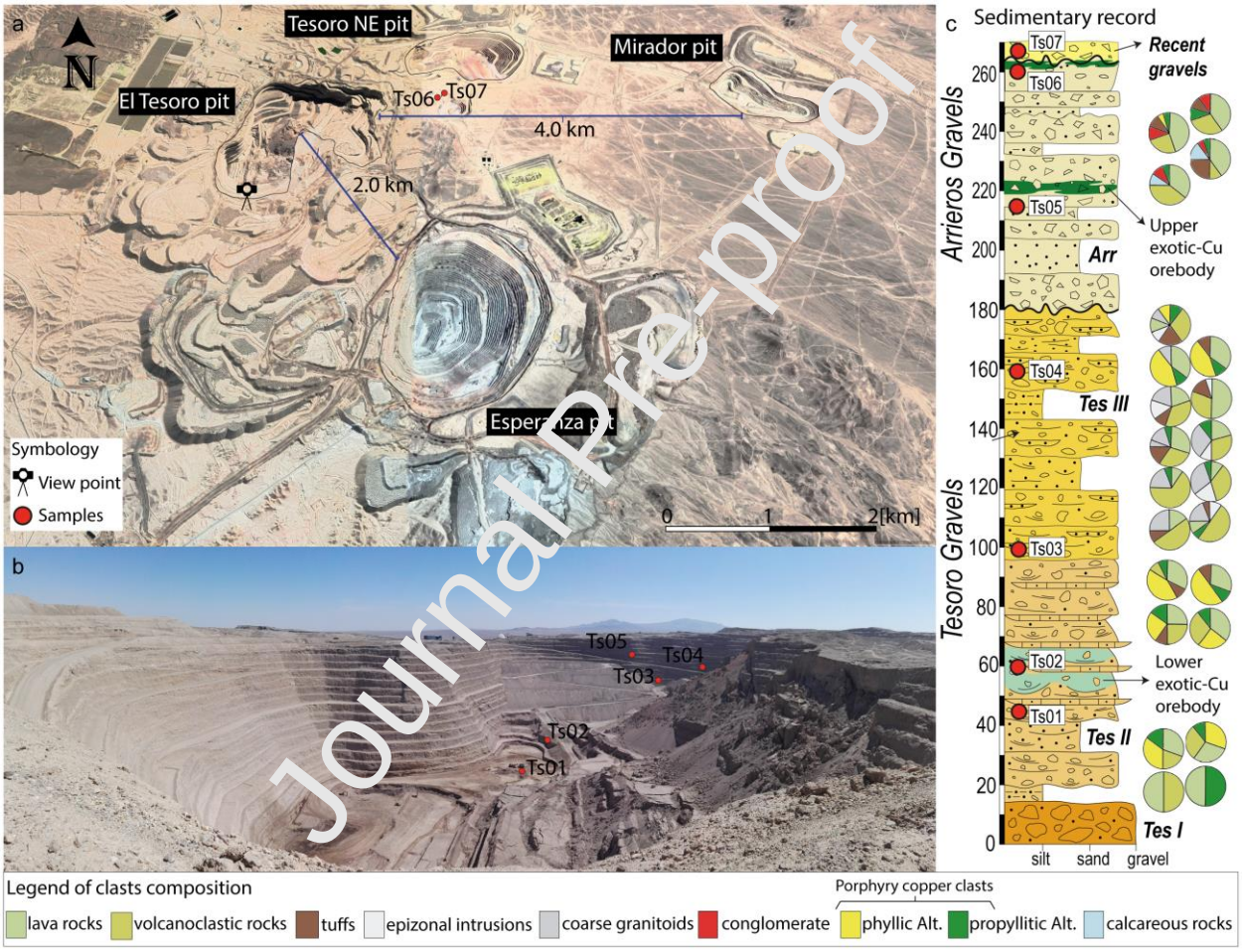

Fig. 2. Location of the mines of Centinela District, sampling of the gravel units and sedimentary record of the El Tesoro pit. **a** Location of El Tesoro and Tesoro NE copper exotic deposits and Esperanza and Mirador copper porphyry deposits and sampling of gravel unit. **b** Picture of El Tesoro Pit (taken from south to north) and sampling of gravel units. **c** Sedimentary

record of the El Tesoro pit (Modified from Fernández-Mort et al., 2018), clast content (Riquelme et al., 2018) and sampling position in stratigraphic column (Tes I: Tesoro I gravels, Tes II: Tesoro II gravels, Tes III: Tesoro III gravels and Arr: Arrieros gravels).

Fig. 3. Transmitted light (left) and cathodoluminescence (right) microscopic images of representative zircon grains collected from studied gravel units**. a** Ts01 (06, 11 and 15 grains). **b** Ts02 (02, 03 and 15 grains). **c** Ts03 (06, 08 and 13 grains). **d** Ts04 (09, 11 and 13 grains). **e** Ts05

(04, 06 and 15 grains). **f** Ts06 (01, 04 and 14 grains). **g** Ts07 (04, 07 and 14 grains). The white circles represent the size and position of the ablation into the grains for trace element measurements. 'Pr' represents the type of prismatic form, and 'Py' the type of pyramidal form. 'R' and 'S' represent the roundness and aspect ratio of the grain, respectively. Ts01 and Ts02: Tesoro II gravels, Ts03 and Ts04: Tesoro III gravels, Ts05 and Ts06: Arrieros gravels and Ts07: Recent gravels.

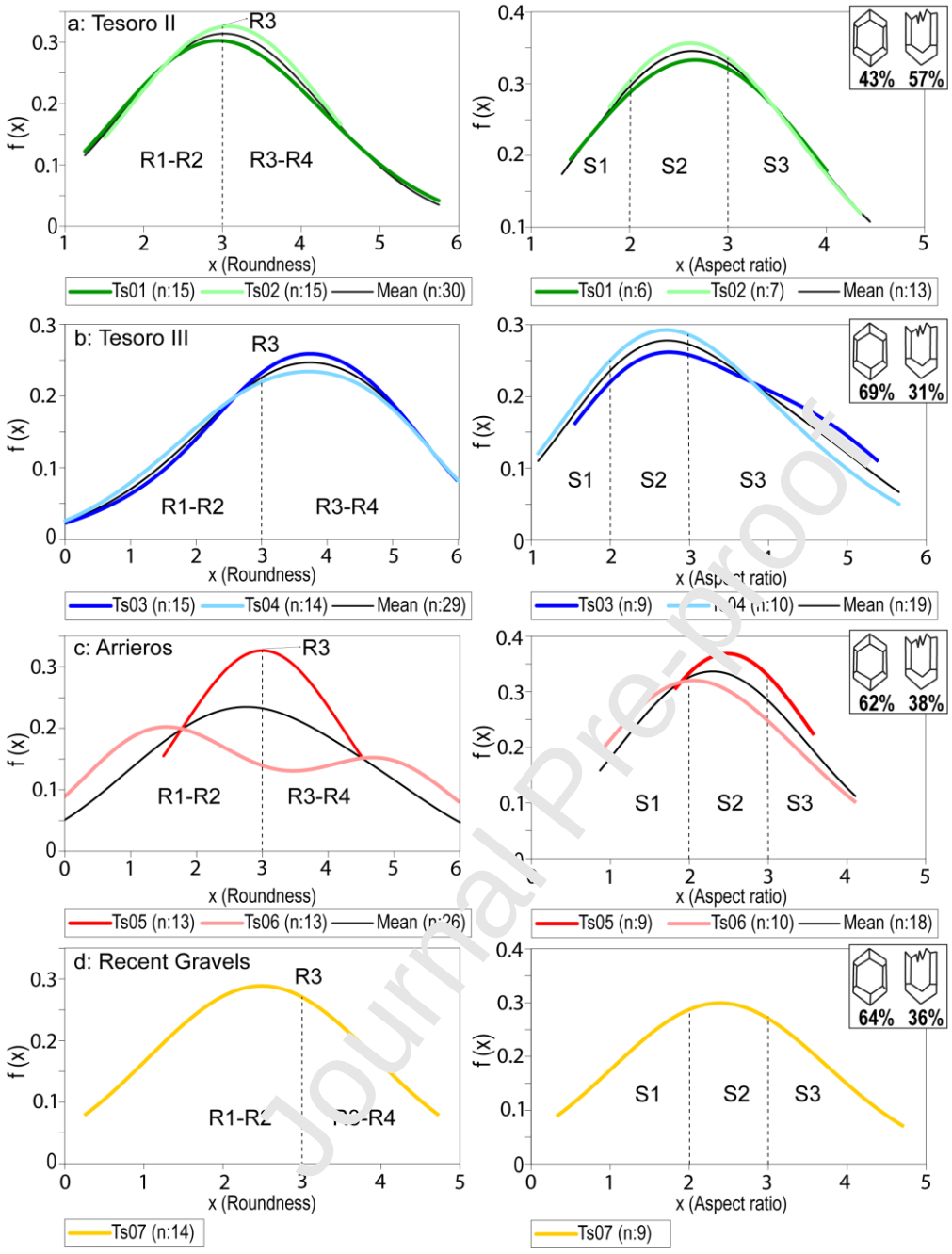

Fig. 4. Kernel density plots of roundness and aspect ratio (length/width) of detrital zircons from the sedimentary record of Centinela District. **a** Tesoro II gravels. **b** Tesoro III gravels. **c** Arrieros gravels. **d** Recent gravels. Percentage of fractured and non-fractured zircons (right upper corner). S1: aspect ratio <2, S2: aspect ratio between 2 and 3, and S3: aspect ratio >3. n, number of analysed crystals.

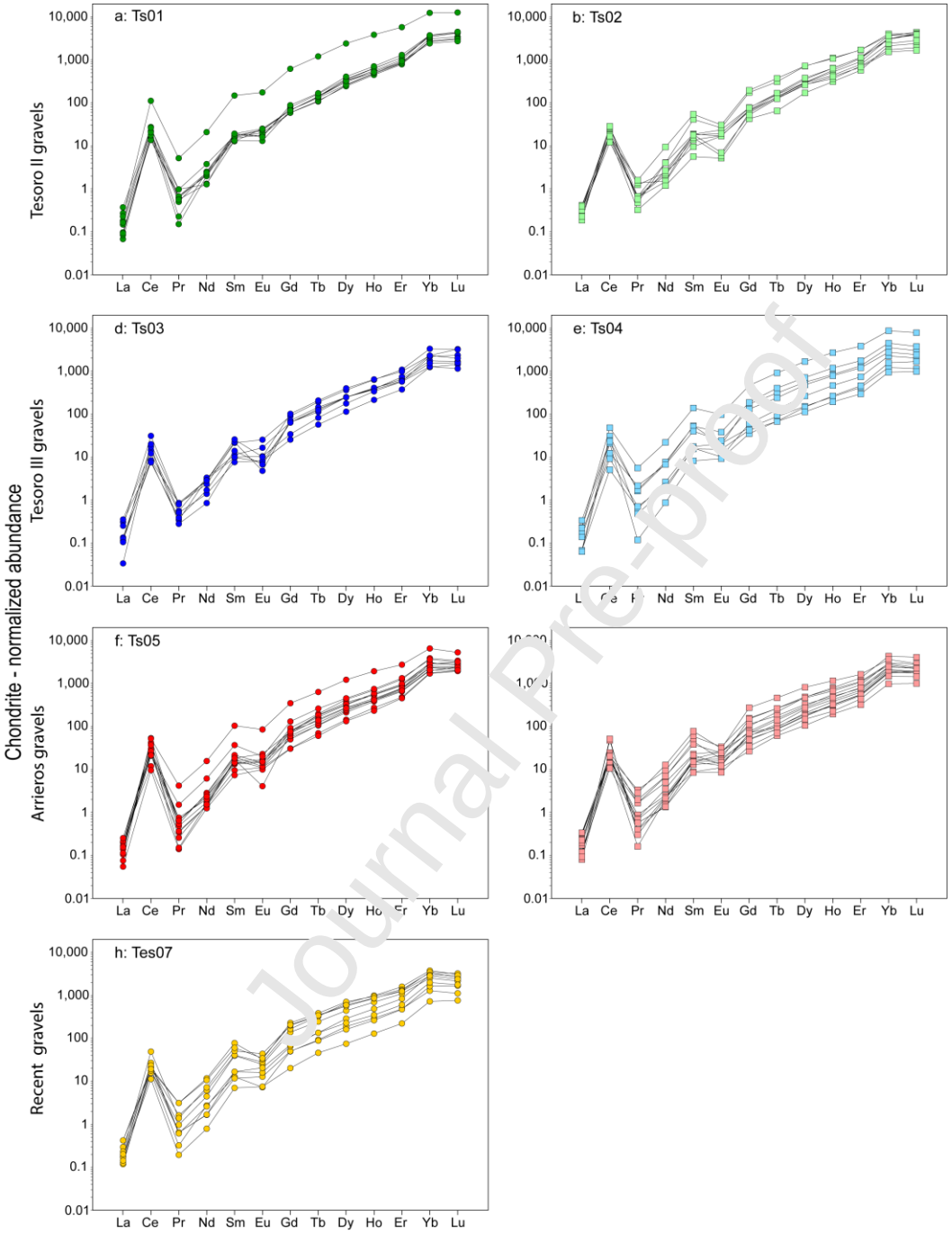

Fig. 5. Chondrite-normalised REE patterns for detrital zircons from sedimentary record of Centinela District**. a** and **b** Tesoro II gravels. **c** and **d** Tesoro III gravels. **e** and **f** Arrieros gravels. **h** Recent gravels. Chondrite values are from McDonough and Sun (1995).

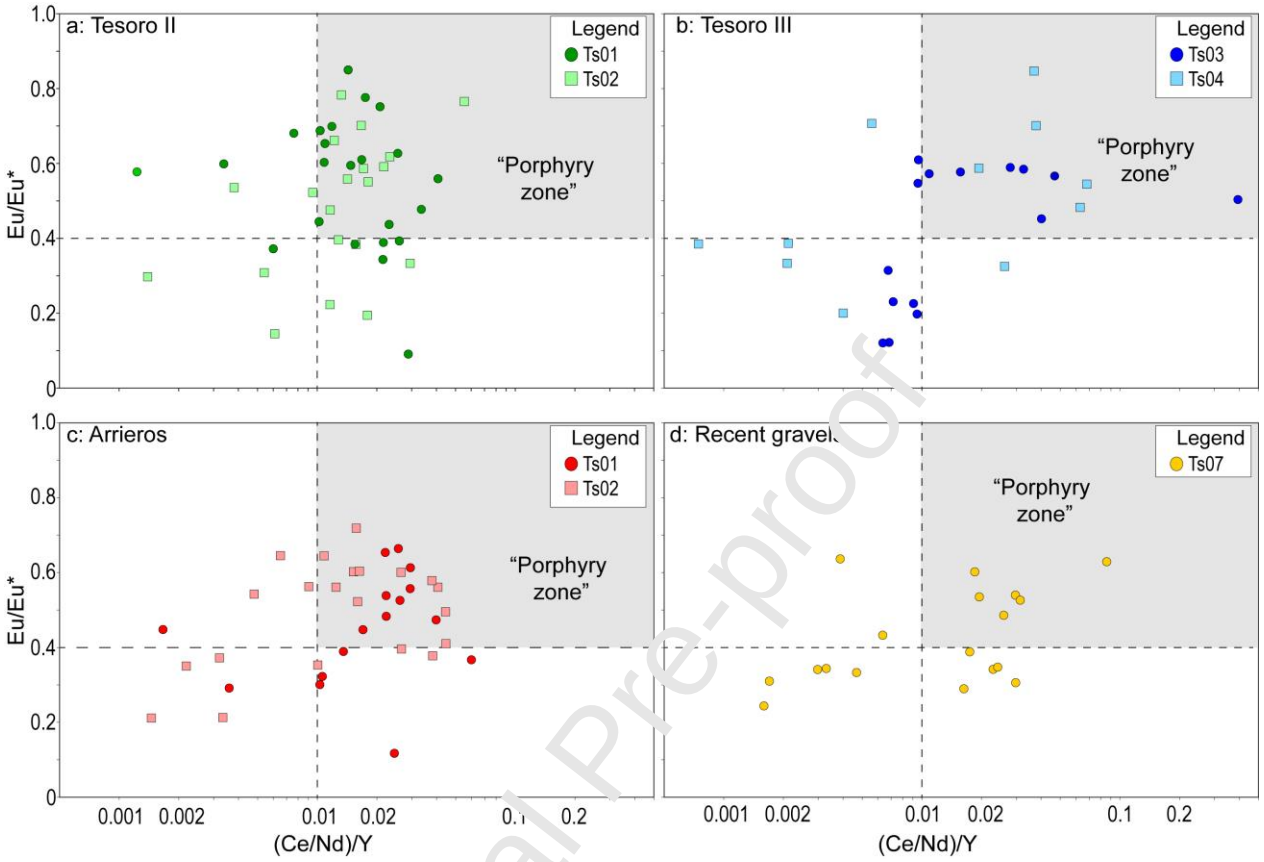

Fig. 6. Zircon (Ce/Nd)/Y vs. Eu/Eu* ratio plot. **a** Tesoro II gravels. **b** Tesoro III gravels. **c** Arrieros gravels. **d** Recent gravels. The Eu anomalies (Eu/Eu*) were calculated from the normalised values of the Sm and Gd concentrations. The Eu/Eu* ratio is defined as $Eu_N/(Sm_N \times Gd_N)^{1/2}$, where the abundance of the elements was normalised to the chondrite values of McDonough and Sun (1995). The dashed vertical and horizontal lines separate fertile from non-fertile fields for porphyry copper deposits worldwide; fertile intrusions have Ce/Nd)/Y >0.01 and Eu/Eu* >0.4 (Ballard et al., 2002; Dilles et al., 2015; Shen et al., 2015; Lu et al., 2016; Pizarro et al., 2020; Lee et al., 2021).

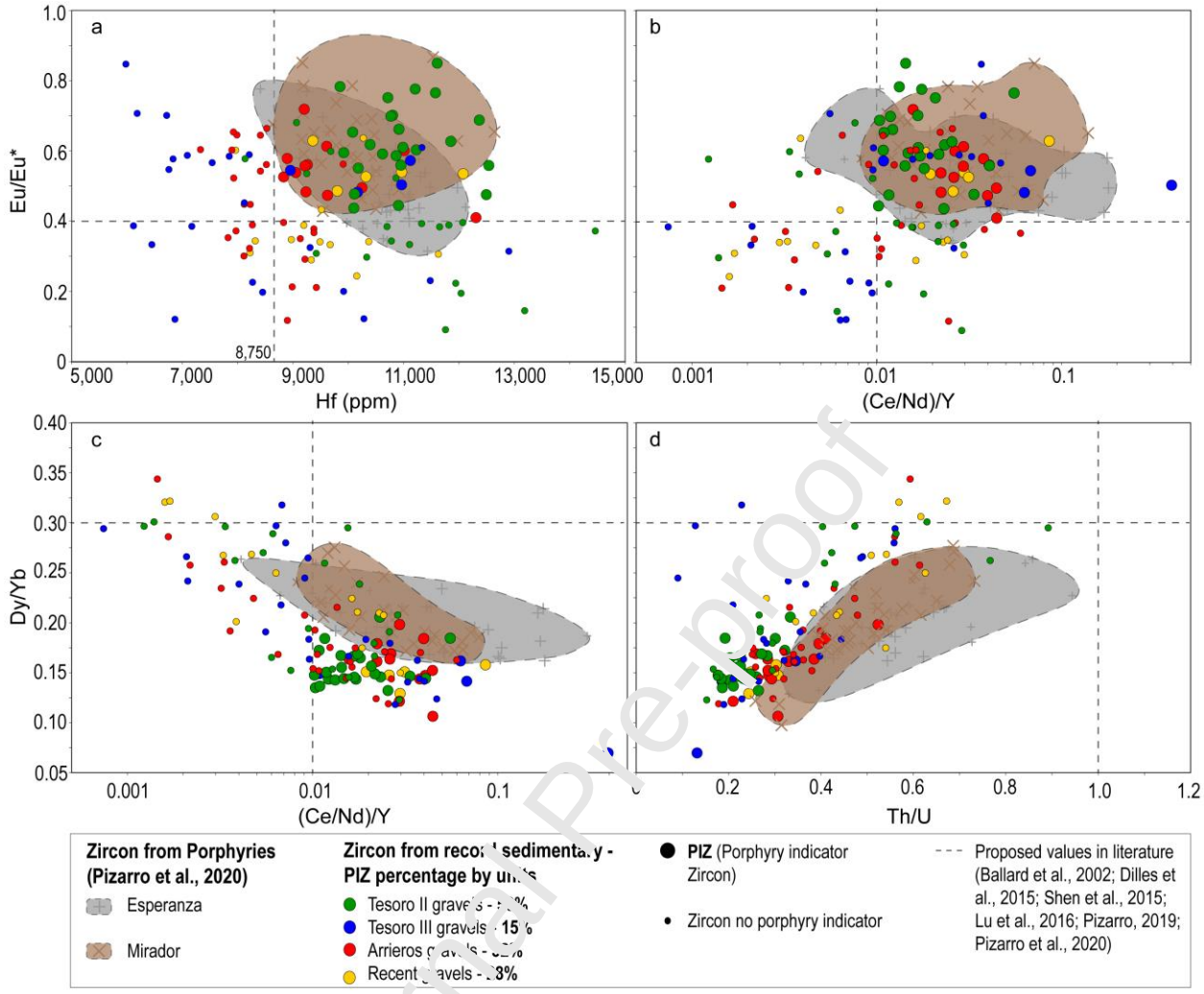

Fig. 7. Trace elements measured in detrital zircons from sedimentary record of Centinela District and zircons from nearby porphyry copper deposits. Sedimentary units: Tesoro II gravels, Tesoro III gravels, Arrieros gravels and Recent gravels. Porphyry copper deposits: Esperanza and Mirador (Modified from Pizarro et al., 2020). **a** Zircon Hf (ppm) vs. Eu/Eu*. **b** Zircon (Ce/Nd)/Y vs. Eu/Eu*. **c** Zircon (Ce/Nd)/Y vs. Dy/Yb. **d** Th/U vs. Dy/Yb. Porphyry indicator zircon (PIZ: Hf >8,750 (ppm), Cd/Nd >1, Eu/Eu* >0.4, 10,000×(Eu/Eu*)/Y >1, (Ce / Nd)/Y >0.01, Dy/Yb <0.3 and 0.1< Th/U <1. The fine dashed vertical and horizontal lines separate fertile from non-fertile fields for porphyry copper deposits worldwide (Ballard et al., 2002; Dilles et al., 2015; Shen et al., 2015; Lu et al., 2016; Pizarro et al., 2020).

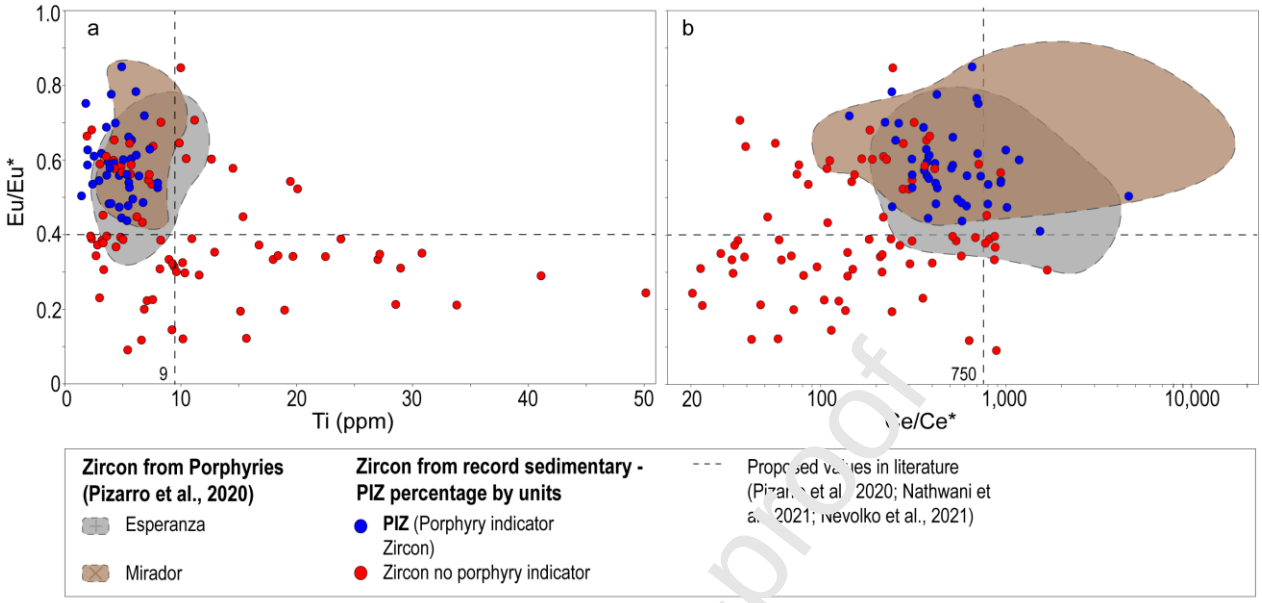

Fig. 8. Trace elements measured in detrital zircons from sedimentary record of Centinela District and zircons from nearby porphyry copper deposits. Sedimentary units: Tesoro II gravels, Tesoro III gravels, Arrieros gravels and Recent gravels. Porphyry copper deposits: Esperanza and Mirador (Modified from Pizarro et al., 2020). **a** Zircon Ti (ppm) vs. Eu/Eu*. **b** Zircon Ce/Ce* vs. Eu/Eu*. Porphyry Indicator Zircon (PIZ: Hf >8,750 (ppm), Cd/Nd >1, Eu/Eu* >0.4, 10,000×(Eu/Eu*)/Y >1, (Ce/Nd)/Y >0.01, Dy/Yb <0.3 and 0.1< Th/U <1. The fine dashed vertical and horizontal lines separate fertile from non-fertile fields for porphyry copper deposits worldwide (Pizarro et al., 2020; Nathwani et al., 2021; Nevolko et al., 2021).

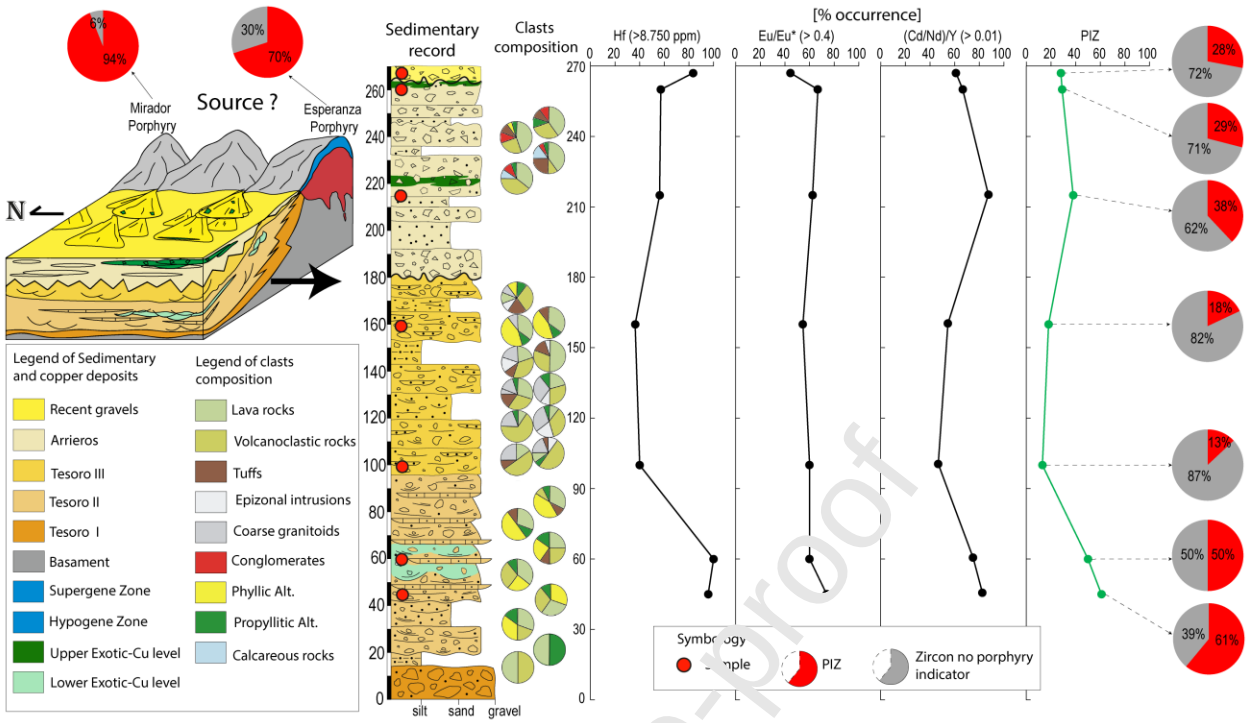

Fig. 9 Relationship between percentage of PIZ and zircon no porphyry indicator in the sedimentary record of Centinela District and the Mirador and Esperanza porphyries. From left to right, the percentage of PIZ of Mirador and Esperanza porphyries (Pizarro et al., 2020), stratigraphic section of the El Tesoro Pit, clast content, curves generated by the occurrence percentage of zircon with Hf concentrations >8,750 (ppm), Eu/Eu* >0.4, (Ce / Nd)/Y >0.01 and percentage of PIZ in the sedimentary record.

Tables and Table Captions

Samples	Zircon state [%]			Aspect Ratio [%]				Roundness [%]						Typological classification of external morphology						
														Prisms morphology			Pyramids morphology			
	Non-fractured	Fractured	n	S1	S2	S3	n	R1	R2	R3	R4	R5	n	{110}	{100}	{110} = {100}	{211}	{101}	{211} = {101}	n
Ts01	40	60	*15*	33	50	17	*6*	0	27	47	27	6	*15*	100	0	0	45	27	27	11
Ts02	47	53	*15*	0	86	14	*7*	0	20	53	27	0	*15*	90	10	0	20	40	40	10
Tesoro II	**43**	**57**	***30***	**15**	**69**	**15**	***13***	**0**	**23**	**50**	**23**	**3**	**30**	**95**	**5**	**0**	**33**	**33**	**33**	**21**
Ts03	60	40	*15*	0	44	56	*9*	7	7	33	33	20	*15*	45	18	36	18	82	0	11
Ts04	71	29	*14*	20	50	30	*10*	7	14	29	21	29	*14*	50	25	25	33	42	25	12
Tesoro III	**69**	**31**	***29***	**11**	**47**	**42**	***19***	**7**	**10**	**31**	**28**	**24**	**29**	**48**	**22**	**30**	**26**	**61**	**13**	**23**
Ts05	62	39	*13*	0	75	25	*8*	0	23	54	23	0	*13*	45	45	9	45	27	27	11
Ts06	69	31	*13*	67	22	22	*10*	30	23	8	8	30	*13*	62	38	0	50	25	25	8
Arrieros	**62**	**38**	**26**	**33**	**44**	**22**	**18**	**15**	**23**	**31**	**15**	**15**	***26***	**53**	**42**	**5**	**47**	**26**	**26**	**19**
Ts07	64	36	*14*	33	44	22	*9*	14	36	36	7	7	*14*	78	22	0	22	44	33	9
Recent gravels	**64**	**36**	**14**	**33**	**44**	**22**	**9**	**14**	**36**	**36**	**7**	**7**	***14***	**78**	**22**	**0**	**22**	**44**	**33**	**9**
	59	**41**	***99***	**27**	**51**	**22**	***52***	**8**	**21**	**37**	**20**	**13**	***99***	**67**	**22**	**11**	**35**	**41**	**24**	**72**

Table 1. Statistical values of petrographic characteristics of detrital zircons from sedimentary record of Centinela District: Tesoro III, Tesoro II, Arrieros and recent gravels**.** Zircon state, sphericity, roundness, and typological classification following Pupin (1980). n: number of grains analysed.

Unit	samples	Statical values	SiO_2 (%)	ZrO_2 (%)	Ti (ppm)	Y (ppm)	Yb (ppm)	Dy (ppm)	Hf (ppm)	Th (ppm)	U (ppm)
Tesoro II gravels	Ts 01	Min	31.5	65.3	1.8	328	186	27	8133	11	53
		Max	32.7	67.3	14.5	5820	1991	591	14462	511	573
		X	31.9	65.9	4.3	1265	571	112	10891	62	165
		x	31.8	65.8	4.0	922.6	509	81	10906	27	119
		σ	0.28	0.45	2.553	1101	342	114	1238	108	130
	Ts 02	Min	31.7	64.3	1.9	357.8	216	36	9247	8	37
		Max	32.4	66.1	15.2	1720	727	183	13186	96	228
		X	32.0	65.3	6.8	920.2	449	88	11103	42	126
		x	32.0	65.3	6.6	832	459	72	10888	34	120
		σ	0.21	0.49	3.465	407.8	151	46	1067	30	47
Tesoro III gravels	Ts 03	Min	31.6	63.1	1.4	146.3	124	9	6756	14	72
		Max	32.3	66.4	19.0	2771	1158	324	12900	217	389
		X	32.0	65.2	6.9	822.8	396	80	9130	54	177
		x	32.0	65.2	4.9	614.7	351	61	8269	26	136
		σ	0.22	0.69	5.112	616.9	255	73	2009	57	98
	Ts 04	Min	31.3	60.5	2.9	277.6	131	21	5978	6	19
		Max	32.3	67.9	18.0	3940	1401	412	10166	160	326
		X	32.0	64.9	8.2	1053	425	100	7640	50	137
		x	32.0	65.0	8.3	548.6	255	41	7089	31	154
		σ	0.27	1.77	4.205	1094	373	116	1614	50	109
Arrieros gravels	Ts 05	Min	31.5	64.2	1.9	402.3	274	33	7922	10	58
		Max	32.5	66.4	15.4	2689	1048	300	9622	114	250
		X	32.1	65.1	7.3	918.3	438	82	8776	50	140
		x	32.2	65.2	6.5	753	376	67	8863	39	141
		σ	0.27	0.54	3.424	528.9	193	62	577.4	31	54
	Ts 06	Min	31.3	60.8	2.2	337.1	158	26	7327	14	50
		Max	33.0	65.4	33.8	1789	698	201	12305	209	653
		X	32.4	64.3	12.3	875.1	392	74	8992	58	164
		x	32.3	64.5	8.6	724.3	341	60	8895	40	105
		σ	0.33	0.99	9.608	430.2	158	45	1170	49	155
Recent gravels	Ts 07	Min	31.8	63.4	2.4	223.5	117	18	7961	16	37
		Max	32.7	66.3	50.2	1839	975	174	12075	307	1018
		X	32.2	65.1	17.6	955.5	429	92	9755	58	164
		x	32.2	65.1	15.5	851.5	423	78	9591	38	92
		σ	0.24	0.95	13.68	449.3	202	48	1098	68	227
		Min	**31.3**	**60.5**	**1.4**	**146.3**	**117**	**9**	**5978**	**6**	**19**
		Max	**33.0**	**67.9**	**50.2**	**5820**	**1991**	**591**	**14462**	**511**	**1018**
		X	**32.1**	**65.1**	**9.2**	**981.3**	**449**	**90**	**9664**	**54**	**154**
		x	**32.1**	**65.2**	**6.1**	**812.5**	**408**	**68**	**9560**	**36**	**120**
		σ	**0.30**	**0.96**	**8.42**	**704.8**	**247**	**75**	**1659**	**63**	**131**

Ce/Ce*	Eu/Eu*	Ce/Nd	(Ce/Nd)/Y	(10000 x Eu/Eu*)/Y	Dy/Yb	Th/U	PIZ by sample	PIZ by unit	PIZ with {110} Prisms
108	0.09	6.3	0.001	0.7	0.132	0.18	61%	56%	100%
998	0.85	35.7	0.041	17.0	0.297	0.89			
472	0.55	16.4	0.017	6.1	0.178	0.29			
382	0.59	12.9	0.016	6.8	0.157	0.24			
243	0.17	8.5	0.010	3.7	0.051	0.15			
34	0.14	2.4	0.001	1.2	0.123	0.15	50%		100%
865	0.78	23.6	0.055	19.6	0.301	0.77			
364	0.48	11.8	0.016	6.6	0.191	0.32			
295	0.53	10.9	0.014	5.5	0.167	0.25			
234	0.19	5.6	0.012	4.9	0.057	0.17			
42	0.12	3.5	0.006	0.8	0.070	0.09	13%	15%	100%
4593	0.61	57.6	0.394	34.4	0.318	0.56			
633	0.41	15.4	0.042	8.1	0.192	0.17			
356	0.50	11.7	0.010	6.1	0.167	0.23			
1129	0.19	14.1	0.098	8.4	0.074	0.14			
33	0.20	2.5	0.001	1.0	0.142	0.19	18%		100%
939	0.85	34.5	0.068	30.5	0.294	0.56			
274	0.50	12.0	0.024	10.7	0.200	0.34			
76	0.48	5.9	0.019	8.6	0.183	0.33			
321	0.20	11.6	0.025	9.7	0.052	0.11			
52	0.12	4.5	0.002	1.1	0.119	0.18	38%	32%	75%
1013	0.66	41.4	0.060	16.5	0.286	0.56			
423	0.45	17.0	0.022	6.3	0.176	0.34			
387	0.46	13.8	0.023	5.9	0.173	0.33			
269	0.15	10.9	0.014	4.1	0.040	0.10			
23	0.21	2.6	0.001	1.2	0.106	0.26	29%		25%
1527	0.72	40.1	0.045	18.1	0.344	0.61			
357	0.49	13.7	0.018	7.5	0.183	0.37			
167	0.54	8.2	0.015	6.9	0.164	0.34			
411	0.14	12.0	0.015	4.8	0.054	0.11			
20	0.24	2.4	0.002	1.6	0.129	0.22	28%	28%	100%
1669	0.64	54.8	0.086	28.1	0.322	0.67			
334	0.42	13.7	0.019	6.4	0.214	0.42			
196	0.37	11.7	0.018	5.7	0.209	0.41			
426	0.13	12.6	0.020	6.1	0.063	0.15			
20	**0.09**	**2.4**	**0.001**	**0.7**	**0.070**	**0.09**	**36%**		**85%**
4593	**0.85**	**57.6**	**0.394**	**34.4**	**0.344**	**0.89**			
411	**0.48**	**14.4**	**0.022**	**7.1**	**0.190**	**0.34**			
311	**0.50**	**11.4**	**0.016**	**6.0**	**0.169**	**0.30**			
494	**0.17**	**10.7**	**0.037**	**5.9**	**0.056**	**0.14**			

Table 2. Statistical values of geochemical measurements of detrital zircons from sedimentary record of Centinela District: Tesoro II, Tesoro III, Arrieros and recent gravels. Min = Minimum value, Max = Maximum value, X = Mean, x = Median, σ = Variance. Eu/Eu* estimated using chondrite values normalised by McDonough and Sun (1995). The Ce/Ce* values were calculated from the method proposed by Nevolko et al. (2021). Percentage of PIZ by samples. A confidence interval of 2σ (95% of the data) was used to eliminate the outlier values, and the values equal to 0 or negative were eliminated.

Appendix and Appendix Captions

Appendix A. Geochemical values measured in detrital zircons (EMPA and LA-ICP-MS) from the Tesoro II, Tesoro III, Arrieros and recent gravels (data table in Excel format). Ce/Ce*(2) and Eu/Eu* were estimated using chondrite values normalised by McDonough and Sun (1995). The Ce/Ce* values were calculated from the method proposed by Nevolko et al. (2021). The Ce/Ce*(1) values were calculated from the method proposed by Nevolko et al. (2021) using chondrite values normalised by McDonough and Sun (1995). Area: c (core) and r (rim).

Appendix B. Petrographic characteristics of detrital zircons from the Tesoro III, Tesoro II, Arrieros and recent gravels (data table in Excel format).

Appendix C. Representative detrital zircon grains from this study shown on roundness and sphericity scales. Roundness ranking ranges from 1 to 5 and appears at the top of each column. The axes used to calculate sphericity are annotated on each grain, and the sphericity <2 was assigned as S1, sphericity between 2 and 3 as S2, and >3 as S3. This methodology was proposed by Shaanan and Rosenbaum (2018).

Acknowledgements

This work was partly funded by ANID (Chilean National Agency of Research and Development) through Doctorados Nacionales scholarship No. 21150393, FONDECYT Postdoctorado Project No. 3210291 and FONDECYT REGULAR Project No. 1220987, by the CESSUR-TelluS Program of CNRS/INSU and IRD (Institut de Recherche pour le Développement, France) through the grant ARTS-IRD No. 862271 K and the Laboratoire Mixte International (LMI) Cuivre et Pediments (COPEDIM), a research program supported by Université Paul Sabatier (Toulouse, France) and Universidad Católica del Norte (Antofagasta, Chile). We thank José Perelló for allowing access and sampling at Centinela District. Also, we acknowledge collaboration with Philippe De Parseval on the EPMA and cathodoluminescence analyses. Additionally, we would like to especially thank Dr. Eduardo Campos for his scientific contribution at all stages of this project. We gratefully acknowledge the editor, Dr. Stefano Albanese, and the constructive comments and suggestions of Dr. Chetan Nathwani and an anonymous reviewer.

References

Ahmed, A. D., Fisher, L., Pearce, M., Escolme, A., Cooke, D. R., Howard, D., Belousov, I., 2020. A microscale analysis of hydrothermal epidote: Implications for the use of laser ablation-inductively coupled plasma-mass spectrometry mineral chemistry in complex alteration environments. Econ. Geol., 115(4), 793-811. https://doi.org/10.5382/econgeo.4705

Andersen, T., 2005. Detrital zircons as tracers of sedimentary provenance: Limiting conditions from statistics and numerical simulation. Chem. Geol. 216(3-4), 249–270. https://doi.org/10.1016/j.chemgeo.2004.11.013

Averill, S.A., 2001. The application of heavy indicator mineralogy in mineral exploration with emphasis on base metal indicators in glaciated metamorphic and plutonic terrains. J. Geol. Soc. Lond. Spec. Publ. 185(1), 69-81. https://doi.org/10.1144/GSL.SP.2001.185.01.04

Averill, S.A., 2011. Viable indicator minerals in surficial sediments for two major base metal deposit types: Ni-Cu-PGE and porphyry Cu. Geochem.: Explor. Environ. Anal. 11(4), 279-291. https://doi.org/10.1144/GSL.SP.2001.185.01.04

Baksheev, I.A., Prokof'ev, V.Y., Zaraisky, G.P., Chitalin, A.F., Yapaskurt, V.O., Nikolaev, Y.N., Petr, L.T., Ekaterina, V.N., Lubov'I, R., Nina, V.G., Kononov, O.V., 2012 Tourmaline as a prospecting guide for the porphyry-style deposits. Eur. J. Mineral. 24(6), 957-979. https://doi.org/10.1127/0935-1221/2012/0024-2241

Ballard, J.R., Palin, M.J., Campbell, I.H., 2002. Relative oxidation states of magmas inferred from Ce (IV)/Ce (III) in zircon: application to porphyry copper deposits of northern Chile. Contrib. Mineral. Petrol. 144, 347–364. https://doi.org/10.1007/s00410-002-0402-5

Bea, F., 1996. Residence of REE, Y, Th and U in granites and crustal protoliths; Implications for the chemistry of crustal melts. J. Petrol. 37, 521–552. https://doi.org/10.1093/petrology/37.3.521

Bell, E.A., Boehnke, P., Harrison, T.M., 2016. Recovering the primary geochemistry of Jack Hills zircons through quantitative estimates of chemical alteration. Geochim. Cosmochim. Acta 191, 187–202. https://doi.org/10.1016/j.gca.2016.07.016

Belousova, E., Griffin, W.L-, O'Reilly, S.Y., Fisher, N.L., 2002. Igneous zircon: trace element composition as an indicator of source rock type. Contrib. Mineral. Petrol. 143(5), 602-622. https://doi.org/10.1007/s00410-002-0364-7

Belousova, E.A., Griffin, W.L., O'Reilly, S.Y., 2005. Zircon crystal morphology, trace element signatures and Hf isotope compositions a tool for petrogenetic modelling: examples from eastern Australian granitoids. J. Petrol. 47(2), 329-353. https://doi.org/10.1093/petrology/egi077

Bouzari, F., Hart, C.J., Bissig, T., Barker, S., 2016. Hydrothermal alteration revealed by apatite luminescence and chemistry: a potential indicator mineral for exploring covered porphyry copper deposits. Econ. Geol. 111(6), 1397-1410. https://doi.org/10.2113/econgeo.111.6.1397

Canil, D., Grondahl, C., Lacourse, T., Pisiak, L.K., 2016. Trace elements in magnetite from porphyry Cu–Mo–Au deposits in British Columbia, Canada. Ore. Geol. Rev. 72, 1116-1128. https://doi.org/10.1016/j.oregeorev.2015.10.007

Chambefort, I., Dilles, J.H., Kent, A.J.R., 2008. Anhydrite-bearing andesite and dacite as a source for sulfur in magmatic-hydrothermal mineral deposits. Geology 36, 719−722. https://doi.org/10.1130/G24920A.1

Chen, X., Huang, W., Chen, L., Zou, S., Zhang, J., Li, K., Liang, H., 2021. Controlling factors of different Late Cretaceous granitoid-related mineralization between western margin of the Yangtze Block and the neighbor Yidun arc. Ore. Geol. Rev. 139, 104554. https://doi.org/10.1016/j.oregeorev.2021.104554

Cherniak, D.J., Hanchar, J.M., Watson, E.B., 1997. Rare-earth diffusion in zircon. Chemical Geology. 134(4), 289-301. https://doi.org/10.1016/S0009-2541(96)00098-8

Cooke, D.R., Agnew, P., Hollings, P., Baker, M., Chang, Z., Wilkinson, J.J., White, N.C., Zhang, L., Thompson, J., Gemmell, J.B., Fox, N., Chen, H., Wilkinson, C.C., 2017. Porphyry indicator minerals (PIMS) and porphyry vectoring and fertility tools (PVFTS)–indicators of mineralization styles and recorders of hypogene geochemical dispersion halos. Dissertation, Decennial Mineral Exploration Conferences.

Cooke, D.R., Baker, M., Hollings, P., Sweet, G., Chang, Z., Danyushevsky, L., Gilbert, S., Zhou, T., White, N., Gemmell, B., Inglis, S., 2014b. New advances in detecting the distal geochemical footprints of porphyry systems - epidote mineral chemistry as a tool for vectoring and fertility assessments. Soc. Econ. Geol. Spec. Publ. 18, 127–152. https://doi.org/10.5382/SP.18.07

Cooke, D.R., Wilkinson, J.J., Baker, M., Agnew, P., Phillips, J., Chang, Z., Chen, H., Wilkinson, C.C., Inglis, S., Holling, P., Zhang, L., Gemmell, B., White, N.C., Danyushevsky, L., Martin, H., 2020. Using mineral chemistry to aid exploration: A case study from the Resolution porphyry Cu-Mo deposit, Arizona. Econ. Geol. 115(4), 813-840. https://doi.org/10.5382/econgeo.4735

Corfu, F., Hanchar, J.M., Hoskin, P.W., Kinny, P., 2003. Atlas of zircon textures. Rev. in Mineral. Geochem. 53(1), 469-500. https://doi.org/10.2113/0530469

Davidson, J., Turner, S., Handley, H., Macpherson, C., and Dosseto, A., 2007, Amphibole "sponge" in arc crust? Geology 35, 787–790. https://doi.org/10.1130/G23637A.1

Dilles, J.H., Kent, A.J.R., Wooden, J.L., Tosdal, R. M., Koleszar, A., Lee, R. G., Farmer, L. P., 2015. Zircon compositional evidence for sulfur-degassing from ore-forming arc magmas. Econ. Geol. 110, 241–251. https://doi.org/10.2113/econgeo.110.1.241

Fedo, C.M., Sircombe, K.N., Rainbird, R.H., 2003. Detrital zircon analysis of the sedimentary record. Rev. Mineral Geochem. 53(1), 277-303. https://doi.org/10.2113/0530277

Ferry, J.M., Watson, E.B., 2007. New thermodynamic models and revised calibrations for the Ti-in-zircon and Zr-in-rutile thermometers. Contrib. Miner. Petrol. 154 (4), 429–437.

Gärtner, A., Linnemann, U., Sagawe, A., Hofmann, M., Ullrich, B., Kleber, A., 2013. Morphology of zircon crystal grains in sediments–characteristics, classifications, definitions. Geol. Saxonica 59, 65–73.

Griffin, W.L., Ryan, C.G., 1995. Trace elements in indicator minerals: area selection and target evaluation in diamond exploration. J. Geochem. Explor. 53(1-3), 311-337. https://doi.org/10.1016/0375-6742(94)00015-4

Griffin, W.L., Powell, W.J., Pearson, N.J., O'Reilly, S.Y., 2008. GLITTER: data reduction software for laser ablation ICP-MS. In: Sylvester P (ed) Laser Ablation–ICP–MS in the earth sciences. Mineral Assoc. Canada Short Course Series 40(2), 204–207

Hanchar, J.M., van Westrenen, W., 2007. Rare earth element behaviour in zircon-melt systems. Elements 3, 37–42. https://doi.org/10.2113/gselements.3.1.37

Hoskin, P.W., Ireland, T.R., 2000. Rare earth element chemistry of zircon and its use as a provenance indicator. Geology 28 (7), 627–630. https://doi.org/10.1130/0091-7613(2000)28<627:REECOZ>2.0.CO;2

Kelley, K.D., Eppinger, R.G., Lang, J., Smith, S.M., Fey, D.L., 2011. Porphyry Cu indicator minerals in till as an exploration tool: example from the giant Pebble porphyry Cu-Au-Mo deposit, Alaska, USA. Geochem.: Explor. Environ. Anal. 11 (4), 321-334. https://doi.org/10.1144/1467-7873/10-IM-041

Kirkland, C.L., Smithies, R.H., Taylor, R.J.M., Evans, N., McDonald, B., 2015. Zircon Th/U ratios in magmatic environs. Lithos. 212, 397-414. https://doi.org/10.1016/j.lithos.2014.11.021

Lee, R.G., Dilles, J.H., Tosdal, R.M., Wooden, J. L., Mazdab, F. K., 2017b. Magmatic evolution of granodiorite intrusions at the El Salvador porphyry copper deposit, Chile, based on trace element composition and U/Pb age of zircons. Econ. Geol. 112, 245–273. https://doi.org/10.2113/econgeo.112.2.245

Lee, R.G., Byrne, K., D'Angelo, M., Hart, C.J., Hollings, P., Gleeson, S.A., Alfaro, M., 2021. Using zircon trace element composition to assess porphyry copper potential of the Guichon Creek batholith and Highland Valley Copper deposit, south-central British Columbia. Miner. Deposita 56(2), 215-238. https://doi.org/10.1007/s00126-020-00961-1

Lee, R.G., Plouffe, A., Ferbey T, Hart, C.J., Hollings, P., Gleeson, S.A., 2021 Recognizing porphyry copper potential from till zircon composition: A case study from the Highland Valley Porphyry district, south-central British Columbia. Econ. Geol. 116(4), 1035-1045. https://doi.org/10.5382/econgeo.4808

Loader, M. A., Nathwani, C. L., Wilkinson, J. J., Armstrong, R. N., 2022. Controls on the magnitude of Ce anomalies in zircon. Geochim. Cosmochim. Acta, 328, 242-257. https://doi.org/10.1016/j.gca.2022.03.024

Loi, A., Dabard, M.P., 1997. Zircon typology and geochemistry in the palaeogeographic reconstruction of the Late Ordovician of Sardinia (Italy). Sediment. Geol. 112(3-4), 263-279. https://doi.org/10.1016/S0037-0738(97)00038-9

Loucks, R.R., 2014. Distinctive composition of copper-ore-forming arc magmas. Aust. J. Earth. Sci. 61(1), 5-16. https://doi.org/10.1080/08120099.2013.865676

Loucks, R.R., Fiorentini, M.L., Henríquez, G.J., 2020. New magmatic oxybarometer using trace elements in zircon. J. Petrol. 61(3) egaa034. https://doi.org/10.1093/petrology/egaa034

Lu, Y.J., Loucks, R.R., Fiorentini, M.L., Yang, Z.M., Hou, Z.Q., 2015. Fluid flux melting generated post-collisional high-Sr/Y copper-ore-forming water-rich magmas in Tibet. Geology 43, 583–586. https://doi.org/10.1130/G36754.1

Lu, Y.J., Loucks, R.R., Fiorentini, M., McCuaig, T.C., Evans, N.J., Yang, Z.M., Hou, Z., Kirkland, C., Parra-Avila, L., Kobussen, A., 2016. Zircon compositions as a pathfinder for porphyry Cu±Mo±Au deposits. Soc. Econ. Geol. Spec. Publ. 19, 329-347. https://doi.org/10.5382/SP.19.13

Lu, Y., Smithies, R.H., Wingate, M.T.D., Evans, N.J., McCuaig, T.C., Champion, D.C., Outhwaite, M., 2019. Zircon fingerprinting of magmatic–hydrothermal systems in the Archean Yilgarn Craton. Geological Survey of Western Australia Report 197, 22.

Matthews, T. J., Loader, M. A., Wilkinson, J. J., Buret, Y., Large, S. J., Birt, E. A., 2023. The Strontian Intrusive Complex: Petrography, Thermobarometry and the Influence of Titanite on Residual Melt Chemistry. J. Petrol. 64(8), egad059. https://doi.org/10.1093/petrology/egad059

Maksaev, V., Zentilli, M., 1999. Fission track thermochronology of the Domeyko Cordillera, northern Chile: Implications for Andean tectonics and porphyry copper metallogenesis. Explor. Mining Geol. 8(1/2), 65-90.

May, G., Hartley, A.J., Stuart, F.M., Chong. G., 1999. Tectonic signatures in arid continental basins: an example from the upper Miocene–Pleistocene, Calama Basin, Andean forearc, northern Chile. Palaeogeogr. Palaeoclimatol. Palaeoecol. 151(1–3), 55–77. https://doi.org/10.1016/S0031-0182(99)00016-4

McDonough, W.F., Sun, S.S., 1995. The composition of the Earth. Chem. Geol. 120(3-4), 223-253. https://doi.org/10.1016/0009-2541(94)00140-4

Morton, A.C., Claoué-Long, J.C., Hallsworth, C.R., 2001. Zircon age and heavy mineral constraints on provenance of North Sea Carboniferous sandstones. Mar. Pet. Geol. 18(3), 319-337. https://doi.org/10.1016/S0264-8172(00)00065-9

Mpodozis, C., Ramos, V.A., 1989. The Andes of Chile and Argentina: Circum-Pacific Council for Energy and Mineral Resources. Earth Sciences Series 11, 59−90.

Mpodozis, C., Cornejo, P., 2012. Cenozoic tectonics and porphyry copper systems of the Chilean Andes. Soc. Econ. Geol. Spec. Publ. 16, 329–360. https://doi.org/10.5382/SP.16.14

Münchmeyer, C., 1996. Exotic deposits: products of lateral migration of supergene solutions from porphyry copper deposits. Soc. Econ. Geol. Spec. Publ. 5, 43–58. https://doi.org/10.5382/SP.05.04

Muñoz, M., Charrier, R., Fanning, C.M., Maksaev, V., Deckart, K., 2012. Zircon trace element and O–Hf isotope analyses of mineralized intrusions from El Teniente ore deposit, Chilean Andes: constraints on the source and magmatic evolution of porphyry Cu–Mo related magmas. J. Petrol. 53(6), 1091-1122. https://doi.org/10.1093/petrology/egs010

Nadoll, P., Mauk, J.L., Leveille, R.A., Koenig, A.E., 2015. Geochemistry of magnetite from porphyry Cu and skarn deposits in the southwestern United States. Miner. Deposita 50(4), 493-515. https://doi.org/10.1007/s00126-014-0539-y

Nakada, S., 1991. Magmatic processes in titanite-bearing dacites, central Andes of Chile and Bolivia. Am. Min. 91(3-4), 548–560.

Nathwani, C.L., Simmons, A.T., Large, S.J., Wilkinson, J.J., Buret, Y., Ihlenfeld, C., 2021. From long-lived batholith construction to giant porphyry copper deposit formation: petrological and zircon chemical evolution of the Quellaveco District, Southern Peru. Contrib. to Mineral Petrol. 76(2), 1-21. https://doi.org/10.1007/s00410-020-01766-1

Nathwani, C. L., Wilkinson, J. J., Brownscombe, W., John, C. M., 2023. Mineral texture classification using deep convolutional neural networks: An application to zircons from porphyry copper deposits. J. Geophys. Res. Solid Earth, 128(2), e2022JB025933. https://doi.org/10.1029/2022JB025933

Neal, L.C., Wilkinson, J.J., Mason, P.J., Chang, Z., 2018. Spectral characteristics of propylitic alteration minerals as a vectoring tool for porphyry copper deposits. J. Geochem. Explor. 184, 179-198. https://doi.org/10.1016/j.gexplo.2017.10.019

Nevolko, P. A., Svetlitskaya, T. V., Savichev, A. A., Vesnin, V. S., Fominykh, P. A., 2021. Uranium-Pb zircon ages, whole-rock and zircon mineral geochemistry as indicators for magmatic

fertility and porphyry Cu-Mo-Au mineralization at the Bystrinsky and Shakhtama deposits, Eastern Transbaikalia, Russia. Ore. Geol. Rev., 139, 104532. https://doi.org/10.1016/j.oregeorev.2021.104532

Pan, L.C., Hu, R.Z., Wang, X.S., Bi, X.W., Zhu, J.J., Li, C., 2016. Apatite trace element and halogen compositions as petrogenetic-metallogenic indicators: Examples from four granite plutons in the Sanjiang region, SW China. Lithos 254, 118-130. https://doi.org/10.1016/j.lithos.2016.03.010

Perelló, J., Brockway, H., Martini, R., 2004. Discovery and geology of the Esperanza porphyry copper-gold deposit, Antofagasta region, northern Chile. Soc Econ Geol Spec Publ 11: 167–186. https://doi.org/10.5382/SP.11.08

Perelló, J., Muhr, R., Mora, R., Martinez, E., Brockway, H., Swaneck, T., Artal, J., Mpodozis, C., Münchmeyer, C., Clifford, J., Acuña, E., Valenzuela, D., Argandoña, R., 2010. Wealth creation through exploration in a mature terrain: The case history of the Centinela district, northern Chile. Soc. Econ. Geol. Spec. Publ. 15,229–252. https://doi.org/10.5382/SP.15.1.13

Petrov, O.V., Khanchuk, A.I., Ivanov, V.V., Shatov, V.V., Seltmann, R., Dolgopolova, A.V., Alenicheva, A.A., Molchanov, A.V., Terekhov, A.V., Leontev, V.I., Belyatsky, B.V., Rodionov, N.V., Sergeev, S.A., 2021. Porphyry indicator zircons (PIZ) and geochronology of magmatic rocks from the Malmyzh and Pony Cu-Au porphyry ore fields (Russian Far East). Ore Geol. Rev. 139: 104491. https://doi.org/10.1016/j.oregeorev.2021.104491

Piccoli, P., Candela, P., Rivers, M., 2000. Interpreting magmatic processes from accessory phases: Titanite—a small-scale recorder of largescale processes. Earth Environ. Sci. Trans. R. Soc. Edinb. 91(1-2), 257-267.

Pisiak, L.K., Canil, D., Lacourse, T., Plouffe, A., Ferbey, T., 2017. Magnetite as an indicator mineral in the exploration of porphyry deposits: a case study in till near the Mount Polley Cu-Au deposit, British Columbia, Canada. Econ. Geol. 112(4), 919-940. https://doi.org/10.2113/econgeo.112.4.919

Pizarro, H. 2019. Trazadores mineralógicos como indicadores de denudación de sistemas mineralizados tipo pórfido cuprífero en el relleno sedimentario de cuencas adyacentes, Desierto de Atacama, Chile. Doctoral dissertation, PhD thesis, Universidad Católica del Norte–Université Paul Sabatier, Toulouse III.

Pizarro, H. Rousse, S., Riquelme, R., Veloso, E., Campos, E., González, R., Bissig, T., Carretier, S., Fernández-Mort, A., Muñoz, S., 2019. The origin of the magnetic record in Eocene-Miocene coarse-grained sediments deposited in hyper-arid/arid conditions: Examples from the Atacama Desert. Palaeogeogr. Palaeoclimatol. Palaeoecol. 516, 322-335. https://doi.org/10.1016/j.palaeo.2018.12.005

Pizarro, H., Campos, E., Belzari, F., Rousse, S., Bissig, T., Gregoire, M., Riquelme, R., 2020. Porphyry indicator zircons (PIZs): Application to exploration of porphyry copper deposits. Ore. Geol. Rev. 126, 103771. https://doi.org/10.1016/j.oregeorev.2020.103771

Pouchou, J.L., Pichoir, F., 1985. PAP'j (rZ) procedure for improved quantitative microanalysis. in "Microbeam analysis", JT Armstrong, ed. San Francisco Press, San Francisco, CA 104, 106

Pupin, J.P., 1980. Zircon and granite petrology. Contrib. Mineral Petrol. 73(3), 207-220. https://doi.org/10.1007/BF00381441

Rabbia, O.M., Hernández, L.B., French, D.H., King, R.W., Ayers, J.C., 2009. The El Teniente porphyry Cu-Mo deposit from a hydrothermal rutile perspective. Miner. Deposita 44, 849–866. https://doi.org/10.1007/s00126-009-0252-4

Rezeau, H., Moritz, R., Wotzlaw, J. F., Hovakimyan, S., & Tayan, R., 2019. Zircon petrochronology of the Meghri-Ordubad pluton, Lesser Caucasus: Fingerprinting igneous processes and implications for the exploration of porphyry Cu-Mo deposits. Econ. Geol. 114(7), 1365-1388. https://doi.org/10.5382/econgeo.4671

Richards, J.P., 2003. Tectono-magmatic precursors for porphyry Cu-(Mo-Au) deposit formation. Econ. Geol. 98(8), 1515-1533. https://doi.org/10.2113/gsecongeo.98.8.1515

Richards, J.P., 2011. High Sr/Y arc magmas and porphyry Cu±Mo±Au deposits: just add water. Econ. Geol. 106(7), 1075-1081. https://doi.org/10.2113/econgeo.106.7.1075

Richards, J.P., 2015. The oxidation state, and sulfur and Cu contents of arc magmas: implications for metallogeny. Lithos 233, 27-45. https://doi.org/10.1016/j.lithos.2014.12.011

Richards, J.P., Boyce, A.J., Pringle, M.S., 2001. Geologic evolution of the Escondida area, northern Chile: A model for spatial and temporal localization of porphyry Cu mineralization. Econ. Geol. 96(2), 271-305. https://doi.org/10.2113/gsecongeo.96.2.271

Richards, J. P., Kerrich, R., 2007. Special paper: adakite-like rocks: their diverse origins and questionable role in metallogenesis. Econ. Geol. 102(4), 537-576. https://doi.org/10.2113/gsecongeo.102.4.537

Richards, J.P., Spell, T., Rameh, E., Razique, A., Fletcher, T., 2012. High Sr/Y magmas reflect arc maturity, high magmatic water content, and porphyry Cu±Mo±Au potential: Examples

from the Tethyan arcs of central and eastern Iran and western Pakistan. Econ. Geol. 107(2), 295-332. https://doi.org/10.2113/econgeo.107.2.295

Riquelme, R., Tapia, M., Campos, E., Mpodozis, C., Carretier, S., González, R., Muñoz, S., Fernández-Mort, A., Sanchez, C., Marquardt, C., 2018. Supergene and exotic Cu mineralization occurs during periods of landscape stability in the Centinela Mining District, Atacama Desert. Basin. Res. 30(3), 395–425. https://doi.org/10.1111/bre.12258

Rubatto, D., 2002. Zircon trace element geochemistry: partitioning with garnet and the link between U–Pb ages and metamorphism. Chem. Geol. 184(1-2), 123-138. https://doi.org/10.1016/S0009-2541(01)00355-2

Russell, R.D., 1955. Effects of transportation on sedimentary particles. Recent Marine Sediments, Parker D. Trask https://doi.org/10.2110/pec.55.04.0032

Russell, J.K. Dipple, G.M., Lang, J.R., Lueck, B., 1999. Major-element discrimination of titanium andradite from magmatic and hydrothermal environments: An example from the Canadian Cordillera. Eur. J. Mineral 11, 929–935.

Sanchez, C., Brichau, S., Riquelme, R., Carretier, S., Bissig, T., Lopez, C., Mpodozis, C., Campos, E., Regards, V., Hérail, G., Marquardt, C., 2018. Exhumation history and timing of supergene copper mineralisation in an arid climate: New thermochronological data from the Centinela District, Atacama, Chile. Terra Nova 30(1), 78-85. https://doi.org/10.1111/ter.12311

Scheuber, E., Reutter, K.J., 1992. Magmatic arc tectonics in the Central Andes between 21° and 25°. Tectonophysics 205(1–3), 127–140. https://doi.org/10.1016/0040-1951(92)90422-3

Scott, K.M., 2005. Rutile geochemistry as a guide to porphyry Cu-Au mineralization, Northparkes, New South Wales, Australia. Geochem.: Explor. Environ. Anal. 5, 247–253. https://doi.org/10.1144/1467-7873/03-055

Scott, R.A., Smyth, H.R., Morton, A.C., Richardson, N., 2014. Sediment provenance studies in hydrocarbon exploration and production. J. Geol. Soc. Lond. Spec. Publ. 386, 1-6. https://doi.org/10.1144/SP386

Seedorff, E., Dilles, J.H., Proffett, Jr J.M., Einaudi, M.T., Zurcher, L., Stavast, W.J.A, Johnson, D.A., Barton, M.D., 2005. Porphyry deposits: Characteristics and origin of hypogene features. Econ. Geol. 100th Anniversary Volume, 251−298. https://doi.org/10.5382/AV100.10

Shaanan, U., Rosenbaum, G., 2018. Detrital zircons as palaeodrainage indicators: Insights into southeastern Gondwana from Permian basins in eastern Australia. Basin Res. 30, 36-47. https://doi.org/10.1111/bre.12204

Shen, P., Hattori, K., Pan, H., Jackson, S., Seitmuratova, E., 2015. Oxidation condition and metal fertility of granitic magmas: Zircon trace-element data from porphyry Cu deposits in the Central Asian Orogenic Belt. Econ. Geol. 110(7), 1861-1878. https://doi.org/10.2113/econgeo.110.7.1861

Sillitoe, R.H., 2005. Supergene oxidized and enriched porphyry copper and related deposits. Econ. Geol. 100th Anniversary Volume 29:723–768. https://doi.org/10.5382/AV100.22

Sillitoe, R. H., 2010. Porphyry copper systems. Econ. Geol. 105(1), 3-41. https://doi.org/10.2113/gsecongeo.105.1.3

Sun, W., Wang, J.T., Zhang, L.P., Zhang, C.C., Li, H., Ling, M.X., Ding, X., Li, C.Y., Liang, H.Y., 2017. The formation of porphyry copper deposits. Acta Geochimica, 361, 9-15. https://doi.org/10.1007/s11631-016-0132-4

Surour, A.A., El-Kammar, A.A., Arafa, E.H., Korany, H.M., 2003. Dahab stream sediments, southeastern Sinai, Egypt: a potential source of gold, magnetite and zircon. J. Geochem. Explor. 77(1), 25-43. https://doi.org/10.1016/S0375-6742(02)00268-6

Thomas, W.A., 2011. Detrital-zircon geochronology and sedimentary provenance. Lithosphere 3(4), 304-308. https://doi.org/10.1130/RF.L001.1

Townley, B.K., Hérail, G., Maksaev, V., Palacios, C., de Parseval, P., Sepulveda, F., Orellana, R., Rivas, P., Ulloa, C., 2003. Gold grain morphology and composition as an exploration tool: application to gold exploration in covered areas. Geochem.: Explor. Environ. Anal. 3(1), 29-38. https://doi.org/10.1144/1467-787302-042

Vavra, G., 1994. Systematics of internal zircon morphology in major Variscan granitoid types. Contrib. Mineral Petrol. 117(4), 331-344. https://doi.org/10.1007/BF00307269

Vermeesch, P., 2004. How many grains are needed for a provenance study?. Earth Planet Sci. Lett. 224 (3-4), 441-451. https://doi.org/10.1016/j.epsl.2004.05.037

Wang, X.C., Li, X.H., Li, Z.X., Li, Q.L., Tang, G.Q., Gao, Y.Y., Zhang, Q.R., Liu, Y., 2012. Episodic Precambrian crust growth: evidence from U–Pb ages and Hf–O isotopes of zircon in the Nanhua Basin, central South China. Precambrian Res. 222, 386-403. https://doi.org/10.1016/j.precamres.2011.06.001

Wilkinson, J.J., Chang, Z., Cooke, D.R., Baker, M.J., Wilkinson, C.C., Inglis, S., Chen, H., Gemmell, J.B., 2015. The chlorite proximitor: A new tool for detecting porphyry ore deposits. J. Geochem. Explor. 152, 10-26. https://doi.org/10.1016/j.gexplo.2015.01.005

Xie, S., Wu, Y., Zhang, Z., Qin, Y., Liu, X., Wang, H., Qin, Z., Liu, Q., Yang, S., 2012. U–Pb ages and trace elements of detrital zircons from Early Cretaceous sedimentary rocks in the Jiaolai Basin, north margin of the Sulu UHP terrane: Provenances and tectonic implications. Lithos 154, 346-360. https://doi.org/10.1016/j.lithos.2012.08.002

Yang, S., Zhang, F., Wang, Z., 2012. Grain size distribution and age population of detrital zircons from the Changjiang (Yangtze) River system, China. Chem. Geol. 296, 26-38. https://doi.org/10.1016/j.chemgeo.2011.12.016

Zheng, B., Mou, C., Wang, X., Chen, T., 2021. U-Pb ages, trace elements and Hf isotopes of detrital zircons from the late Permian-early Triassic sedimentary succession in the northern Yangtze Block, South China: Implications for the reconstruction of the South China Block in Pangea. J. Asian Earth Sci. 206, 104609. https://doi.org/10.1016/j.jseaes.2020.104609

Zoleikhaei, Y., Frei, D., Morton, A., Zamanzadeh, S.M., 2016. Roundness of heavy minerals (zircon and apatite) as a provenance tool for unraveling recycling: A case study from the Sefidrud and Sarbaz rivers in N and SE Iran. Sediment Geol. 342, 106-117. https://doi.org/10.1016/j.sedgeo.2016.06.016

Zou, X., Qin, K., Han, X., Li, G., Evans, N.J., Li, Z., Yang, W., 2019. Insight into zircon REE oxy-barometers: A lattice strain model perspective. Earth Planet Sci. Lett. 506, 87-96. https://doi.org/10.1016/j.epsl.2018.10.031

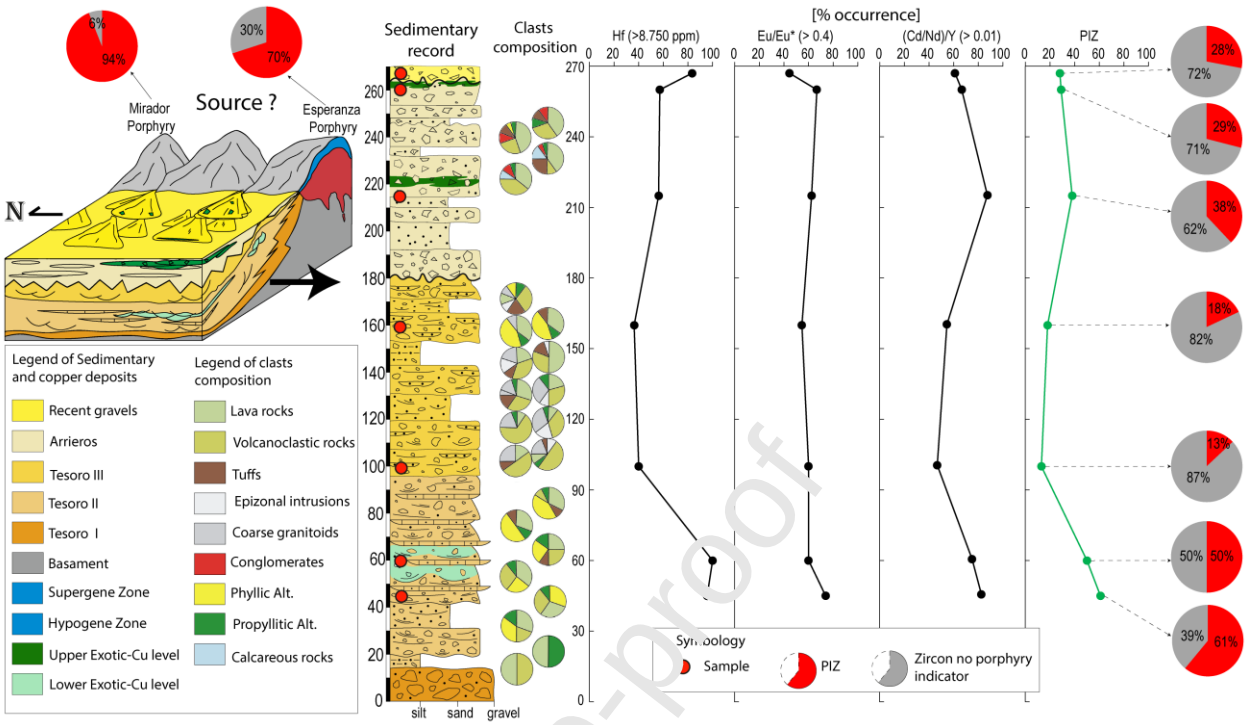

Graphical abstract

Highlights:

1. Group of geochemical indicators summarized as Porphyry Indicator Zircon (PIZ)
2. 36% of zircons found in the gravels of Centinela district correspond to PIZ
3. The gravels with exotic-Cu mineralization have highest concentration of PIZ
4. PIZ in sedimentary records are a good tracer of adjacent copper porphyries
5. PIZ are a promising exploration tool in search for hidden copper porphyries